Kaunas University of Technology

Faculty of Chemical Technology

Synthesis and Properties Investigation of Fluorene-based Electroactive Compounds

Master's Final Degree Project

Rashad Naghizade

Project author

Assoc. Prof. Rasa Keruckienė

Supervisor

Kaunas, 2026

Kaunas University of Technology

Faculty of Chemical Technology

Synthesis and Properties Investigation of Fluorene-based Electroactive Compounds

Master's Degree Final Project

Chemical Engineering (6211EX020)

Rashad Naghizade

Project author

Assoc.Prof. Rasa Keruckienė

Supervisor

Assist.Prof. Monika Čekavičiūtė

Reviewer

Kaunas, 2026

Kaunas University of Technology

Faculty of Chemical Technology

Rashad Naghizade

Synthesis and Properties Investigation of Fluorene-based Electroactive Compounds

Declaration of Academic Integrity

I confirm the following:

1. I have prepared the final degree project independently and honestly without any violations of the copyrights or other rights of others, following the provisions of the Law on Copyrights and Related Rights of the Republic of Lithuania, the Regulations on the Management and Transfer of Intellectual Property of Kaunas University of Technology (hereinafter - University) and the ethical requirements stipulated by the Code of Academic Ethics of the University;

2. All the data and research results provided in the final degree project are correct and obtained legally; none of the parts of this project are plagiarised from any printed or electronic sources; all the quotations and references provided in the text of the final degree project are indicated in the list of references;

3. I have not paid anyone any monetary funds for the final degree project or the parts thereof unless required by the law;

4. I understand that in the case of any discovery of the fact of dishonesty or violation of any rights of others, the academic penalties will be imposed on me under the procedure applied at the University; I will be expelled from the University and my final degree project can be submitted to the Office of the Ombudsperson for Academic Ethics and Procedures in the examination of a possible violation of academic ethics.

Rashad Naghizade

Confirmed electronically

Kaunas University of Technology

Faculty of Chemical Technology

I confirm: Dean of Faculty of Chemical Technology Prof. Dr. Vaida Kitrytė-Syrpa Decree of the Dean No. V25-02-13 2026 May 14	Coordinated with: Head of the Department of Polymer Chemistry and Technology Assoc. Prof. Dr. Audrius Bučinskas 2026 March 4

Master's final degree project

Topic of the project	Synthesis and Properties Investigation of Fluorene-based Electroactive Compounds
Aim of the work and tasks	The aim of this work is to perform the structure-properties investigation of fluorene-based compounds. Tasks: 1. To synthesize six compounds containing spirobifluorene, dimethylfluorene, phenylcarbazole, phenyldibenzofuran, and terthiophene moieties; 2. To investigate their thermal, photophysical, and electrochemical properties; 3. To create a technological scheme for the production of 6,6'-(9,9-dimethyl-9H-fluorene-2,7-diyl)bis(4-phenyldibenzo[b,d]furan).
Requirements and conditions	There must be all mandatory parts in the final project as specified by „Methodological requirements for preparation and defence of final degree projects for bachelor‘s programme Chemical technology and engineering and master‘s programme Chemical engineering“ approved by Dean Decree No. V25-02-10 (March 6 2024).

Supervisor	Assoc.Prof. Rasa Keruckienė	04-03-2026
	(position, name, surname, signature)	(date)

Task received: Rashad Naghizade 04-03-2026

(name, surname) (signature, date)

Rashad Naghizade. Synthesis and Properties Investigation of Fluorene-based Electroactive Compounds. Master's Final Degree Project supervisor Assoc.Prof. Rasa Keruckienė; Faculty of Chemical Technology; Chemical Engineering; Kaunas University of Technology.

Study field and area (study field group): Engineering Sciences, Chemical Engineering.

Keywords: spirobifluorene, dimethylfluorene, dibenzofuran, carbazole, thiophene, OLED

Kaunas, 2026. 62 pages.

Summary

Electroactive organic materials are employed in optoelectronic applications involving organic light-emitting diodes. Spirobifluorene, dimethylfluorene, phenylcarbazole, phenyldibenzofuran, and terthiophene were selected for new electroactive materials synthesis. The compounds were synthesized using Suzuki coupling reactions. The structures of the synthesized materials were confirmed by nuclear magnetic resonance spectroscopy and mass spectroscopy.

The thermal characteristics of the synthesized materials were studied by differential scanning calorimetry (DSC) and thermogravimetric analysis (TGA). All the synthesized materials characterized by high thermal stability, with a decomposition temperature range of 430 °C to 483 °C at 5% weight loss, glass transition temperatures were recorded in the range of 120-183 °C.

The cyclic voltammetry (CV) was used to estimate the ionization potentials of the synthesized materials. They exhibited comparable findings, varying from 5.38 to 6.28 eV

The synthesized spirobifluorene and dimethylfluorene core compounds show luminescence in the blue region, whereas the terthiophene core compounds emit light in the yellow region. The photoluminescence quantum yields of the thin film of spirobifluorene, dimethylfluorene, and terthiophene core compounds were up to 46%, and the photoluminescence quantum yields of the solutions of terthiophene core compounds were up to 90%.
The technological scheme for the production of a dibenzofuranyl-disubstituted dimethylfluorene core compound was developed.

Rashad Naghizade. Fluorenilfragmentus turinčių elektroaktyvių junginių sintezė ir savybių tyrimas. Magistro baigiamasis projektas, vadovė Assoc.Prof. Rasa Keruckienė; Cheminės technologijos fakultetas; Chemijos Inžinerija; Kauno technologijos universitetas.

Studijų kryptis ir sritis (studijų krypčių grupė): Inžinerijos mokslai, chemijos inžinerija.

Reikšminiai žodžiai: spirobifluorenas, dimetilfluorenas, dibenzofuranas, karbazolas, tiofenas, OLED

Kaunas, 2026. 62 p.

Santrauka

Elektroaktyvios organinės medžiagos naudojamos optoelektronikos taikymuose, susijusiuose su organiniais šviesos diodais. Spirobifluorenas, dimetilfluorenas, fenilkarbazolas, fenildibenzofuranas ir tertiofenas buvo pasirinkti naujų elektroaktyviųjų medžiagų sintezei. Junginiai buvo susintetinti naudojant Suzuki sujungimo reakcijas. Susintetintų medžiagų struktūros buvo patvirtintos branduolinio magnetinio resonanso spektroskopija ir masių spektrometrija.

Susintetintu medžiagu terminės savybės buvo tirtos diferencinės skenuojamosios kalorimetrijos (DSC) ir termogravimetrinės analizės (TGA) metodais. Visoms susintetintoms medžiagoms buvo būdingas didelis terminis stabilumas, skilimo temperatūros intervalas nuo 430 °C iki 483 °C, esant 5% svorio sumažėjimui, stiklėjimo temperatūros intervalas buvo 120-183 °C.

Susintetintų medžiagų jonizacijos potencialams įvertinti buvo taikyta ciklinė voltamperometrija (VK). Gauti panašūs rezultatai nuo 5.38 iki 6.28 eV

Susintetinti spirobifluoreno ir dimetilfluoreno branduolius turintys junginiai liuminescenciją rodo mėlynojoje srityje, o tertiofeno branduolį turintys junginiai emituoja šviesą geltonojoje srityje. Spirobifluoreno, dimetilfluoreno ir tertiofeno branduolius turinčių junginių plonųjų plėvelių fotoliuminescencijos kvantiniai našumai siekė iki 46%, o tertiofeno junginių tirpalų fotoliuminescencijos kvantiniai našumai siekė iki 90%.

Sukurta dibenzofuranilu disubstituoto dimetilfluoreno branduolį junginio gamybos technologinė schema.

Table of contents

List of figures

List of tables

List of abbreviations and terms

CT – Charge Transfer
CV - cyclic voltammetry
CIJ - Continuous-Stream Inkjet
CDCl3 - chloroform
DSC - differential scanning calorimetry
D-A - donor-acceptor
DoD - Drop-on-Demand
DMF - dimethylformamide
DCM - dichloromethane
DMSO - dimethyl sulfoxide
ETL - electron transport layer
EIL - electron injection layer
EML - emissive layer
EQE - external quantum efficiency
FT-IR - Fourier-Transform Infrared spectroscopy
HTL - hole transport layer
HIL - hole injection layer
HOMO - highest occupied molecular orbital
IQE - internal quantum efficiency
LUMO - lowest unoccupied molecular orbital
MS - mass spectrometry
MW - molecular weight
NMR - nuclear magnetic resonance
OLED - organic light-emitting diode
PLQY - photoluminescence quantum yield
PL - Photoluminescence spectroscopy
RISC - reverse intersystem crossing
SBF - spirobifluorene
TGA - thermogravimetric analysis
TADF - thermally activated delayed fluorescence
THF - tetrahydrofuran
TRPL - Time-resolved photoluminescence
UV - ultraviolet
VTE - vacuum thermal evaporation

Introduction

Low-molar-mass and polymer organic light emitting diodes have attracted considerable attention due to their great potential in large area flat panel displays and solid-state lighting application [1]. Such devices tend to have multilayer device configuration with a hole transport layer, an electron transport layer and an emissive layer, and some of them also have a hole injection and an electron injection layer [2]. The appropriate materials selection for each layer is of great importance. Generally, the molecular structures of hole transport materials usually contain electron-donating moieties, such as carbazole, triarylamine, diphenylamine, N-phenyl-1-naphthylamine, etc. [3]. An organic light-emitting diode (OLED) is composed of at least one organic layer that is put between two electrodes. Electrons and holes are injected from either side of the electrode. When a voltage is applied, both carriers will drift toward the other side in the applied electric field. When both electrons and holes meet in the bulk or at an interface, they recombine to form excitons, which then decay to produce light [4]. However, traditional methods for synthesizing electroactive materials have notable drawbacks such as low reaction yields, longer reaction times, dependence on hazardous, expensive, and moisture-sensitive reagents, and the use of large amounts of reactants. Additionally, these methods often require intense reaction conditions, longer workup procedures, and difficulties in catalyst regeneration. Furthermore, efficiency roll-off and low device stability of OLEDs remain key drawbacks, developing new materials that overcome these issues is vital [5]. In this study, we have designed and synthesized six new electroactive compounds to establish their structure influence on thermal, electrochemical and photophysical properties.

The aim of this work is to perform the structure-properties investigation of fluorene-based compounds.

Tasks

4. To synthesize six compounds containing spirobifluorene, dimethylfluorene, phenylcarbazole, phenyldibenzofuran, and terthiophene moieties;
5. To investigate their thermal, photophysical, and electrochemical properties;
6. To create a technological scheme for the production of 6,6'-(9,9-dimethyl-9H-fluorene-2,7-diyl)bis(4-phenyldibenzo[b,d]furan).

1. Literature survey

1.1. Fundamentals of OLEDs

1.1.1. OLED structure

The OLED device itself is designed as a multilayered structure, commonly represented as a sandwich encompassing various essential layers: electron transport layer (ETL), hole transport layer (HTL), electron injection layer (EIL), hole injection layer (HIL), and the emissive layer (EML) (Figure 1a) [6,7]. In OLED devices, the organic layers are sandwiched within two electrodes: an anode and a cathode, which are positioned on opposite sides [2,6,7]. On the anode side, the HIL is typically employed to promote hole injection (Figure 1b) [6,7]. Indium tin oxide (ITO) is widely used as an anode material [6]. With the aim of initiating the holes into organic layers and acquiring high output and reliability, the transparent and extremely conductive anode must be utilized. On the cathode side, the EIL with an average energy level within that of the ETL and the cathode layer's work function, is incorporated. The electrons are injected into the EML by the cathode layer [2]. Once a bias voltage is introduced throughout the electrodes, holes are injected into the highest occupied molecular orbital (HOMO) of the HIL while the electrons are inserted into the lowest unoccupied molecular orbital (LUMO) of the EIL. Promoted by the external voltage, positive and negative charges are transferred to the EML via HTL and ETL, where they build up across the interfacial barriers to generate excitons [8]. Upon the electrons and holes reaching the EML, they merge to produce molecular excitons [6]. The EML is a layer within the HTL and ETL that emits visible photons. HTL is crucial in OLEDs: it functions as a barrier among the anode and EML. Through chemical interactions or dipole formation, the ETL operates as an interlayer to lower electron-injection barriers at both the cathode and the EML [2]. Furthermore, electron-blocking layer (EBL) and hole-blocking layer (HBL) are commonly integrated in OLEDs to improve the exciton confinement and preserve a uniform charge distribution of holes and electrons by suppressing the charge carrier and exciton leakage from the EML to adjacent layers [6]. In OLED structure, the substrate is a key component; glass is often used as a substrate due to its stability and high glass transition temperature. Additionally, plastic panels, particularly translucent plastic and transparent metal foil, can also be used as substrates [2].

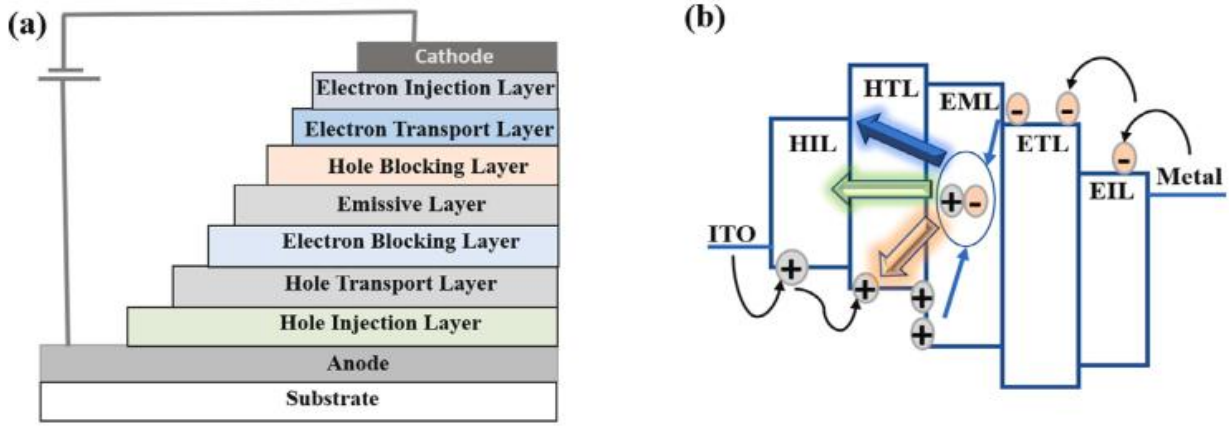

Fig. 1. Multi-layer construction of OLED [2].

Flexible substrates such as metal foils, thin glass sheets, polymer films, paper, and textiles are essential in determining the flexibility of OLEDs. The most widely used substrates for flexible organic devices are polymer films due to their advantages, including high flexibility, transparency, waterproofness, and mechanical robustness. However, OLEDs utilizing fabrics as substrates can be

directly incorporated with clothing for applications such as display, lighting, decoration, sensing, and healthcare [8].

In addition to traditional multilayer devices, advanced designs, particularly tandem OLEDs, have developed as an emerging technology due to their superiorities such as outstanding performance, reliability, and prolonged lifetime. Within these tandem OLEDs, the device efficiency and stability are predominantly determined by the charge generation unit (CGU) [9].

1.1.2. Light emitting mechanism in OLEDs

Fluorescent OLEDs, the initial version of this technology, utilize organic dyes as their luminous emissive materials. However, they are fundamentally restricted by the laws of electron spin statistics, allowing only the radiative transition of singlet excitons to emit fluorescence [10]. In accordance with spin-statistics, only 25% of singlet excitons are formed throughout the hole-electron recombination process (Figure 5a). Fluorescent materials can only use singlet excitons to emit light, while the remaining 75% triplet excitons are dissipated as non-radiative energy due to the limited transition between singlet and triplet states [6,11,12]. For commonly used organic fluorescent materials, their internal quantum efficiency (IQE) is restricted to 25%, and outcoupling efficiency is around 20%. Nevertheless, the inability to harness the energy potential of triplet excitons leads to a significant challenge, restricting the external quantum efficiency (EQE) of fluorescent OLEDs to almost 5% [13]. This insufficient efficiency in exciton conversion contributes to the low performance of OLEDs. In 2022, Xiao et. al. [14] introduced two deep-blue emitters (Figure 2) 2-(4′-(9,9-dimethylacridin-10(9H)-yl)-[1,1′biphenyl]-4-yl)-1-phenyl-1H-phenanthro[9,10-d]imidazole (**DP**) and 10-(4′-(1-phenyl-1H-phenanthro[9,10-d]imidazol-2-yl)-[1,1′-biphenyl]-4-yl-10H-spiro[acridine-9,9′-fluorene]-(**SP**) where neat films of these materials exhibit deep-blue emission at 442 nm and 436 nm accordingly, having photoluminescence quantum yields (PLQY) of 40% (**DP**) and 62% (**SP**).

In trying to break out of this restriction, researchers paid special attention to developing new materials such as phosphorescent heavy metal complexes.

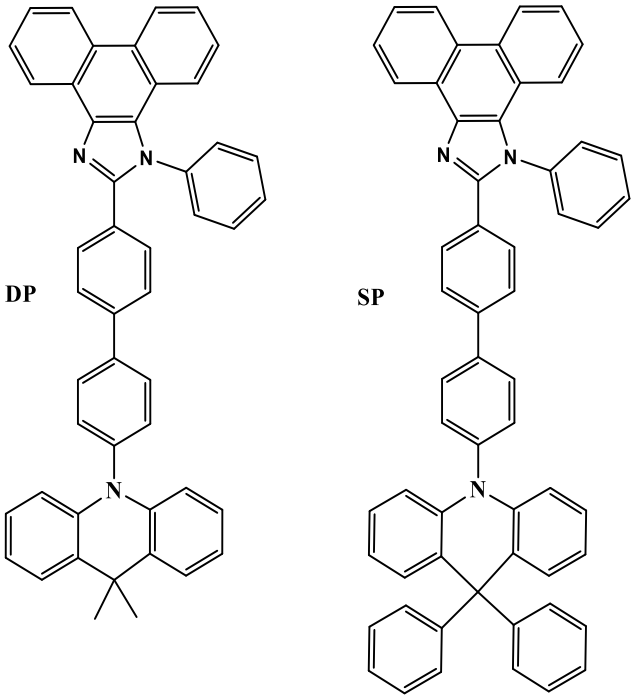

Fig. 2. Chemical structure of **DP** and **SP** [13]

In comparison with fluorescent materials, phosphorescent heavy metal complexes such as iridium, platinum, ruthenium, rhodium, europium, terbium, and osmium have been used to harvest both singlet and triplet excitons through intersystem crossing (ISC) induced by spin-orbital coupling, leading to an internal quantum efficiency up to 100% [15-17]. Consequently, radiative decay from the triplet state to the ground state singlet emerges due to spin-orbit coupling (Figure 5b) [18]. For instance: compound namely cis-Ir(N,C-ppy)2(O,O-THC) (ppy = phenylpyridine) (Figure 3a) emits in the green region at 520 nm, having PLQY of 90% [19], and tetradentate ligand N-(2',6'-difluoro-4-methyl-[2,30-bipyridin]-6-yl)-N-(2,6-dimethylphenyl)-2',6'-difluoro-4-methyl-[2,3'-bipyridin]-6-amine (**XA-H-Pt** and **XA-CH3-Pt**) (Figure 3b-c) white emission material, having 100% PLQY [20].
However, several disadvantages were revealed in the use of phosphorescent emitters. These include that the metal complexes utilized are rare earth metals exhibiting toxicity, high cost, and limited color purity, all of which have enhanced the research on alternative, metal-free materials such as thermally activated delayed fluorescence (TADF) [15,21].

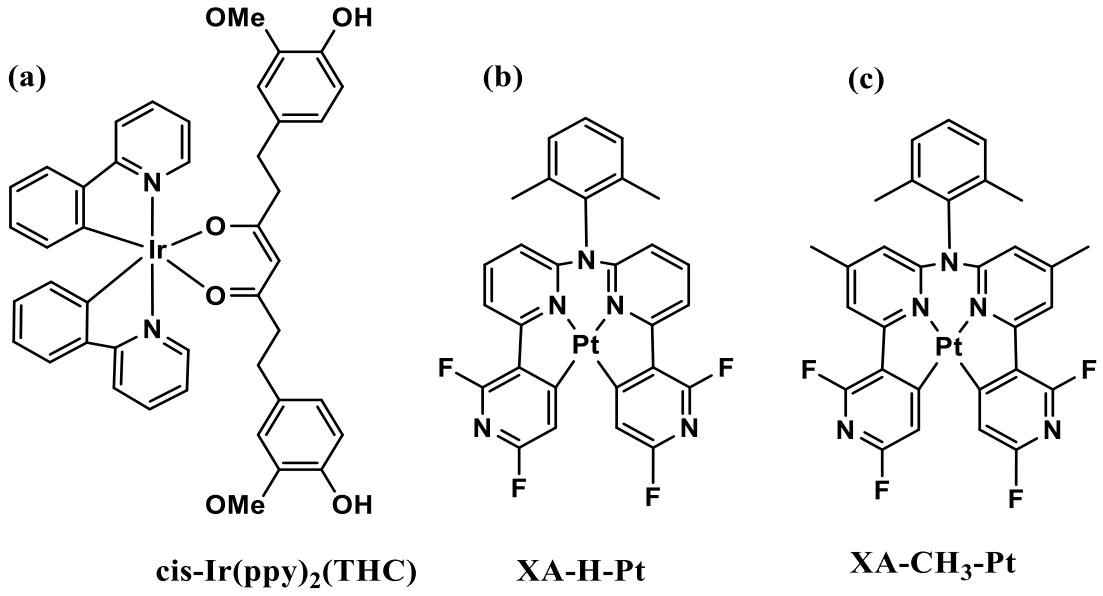

Fig. 3. Structures of **XA-H-Pt, XA-CH3-Pt** and **cis-Ir(N,C-ppy)2(O,O-THC)** [19,20].

TADF has evolved as a transformative strategy in the structure of OLED technology by promoting almost 100% IQE due to the use of both singlet and triplet excitons (Figure 5c) [21-23]. TADF belongs to a type of luminescence that influences thermal energy to transform non-radiative triplet excitons into radiative singlet excitons, efficiently enhancing electroluminescence efficiency [22-24]. The operating mechanism of TADF arises from the ability to convert non-radiative triplet excitons into radiative singlet states enabled by reverse intersystem crossing (RISC), a thermally activated upconversion process from triplet to singlet states [21-24]. This conversion necessitates a small singlet-triplet energy gap to enhance thermal activation, and a well-designed molecular structure maintains spatial separation of the HOMO and LUMO, reducing the energy gap [22,24,25]. The widely used TADF design includes donor-acceptor (D-A) structures where the HOMO (donor side) and LUMO (acceptor side) are spatially separated to decrease the exchange energy and therefore the energy gap [21-23,25].
In 2023, Kothavale et. al. [26] introduced a novel TADF emitter (Figure 4), 6,7-bis(4-(bis(4-(tert-butyl)phenyl)amino)phenyl)-2,3-bis(4-(tert-butyl)phenyl)quinoxaline-5,8-dicarbonitrile (***t*BuTPA-CNQx**), which exhibits pure red emission at 662 nm, having PLQY of 92%.

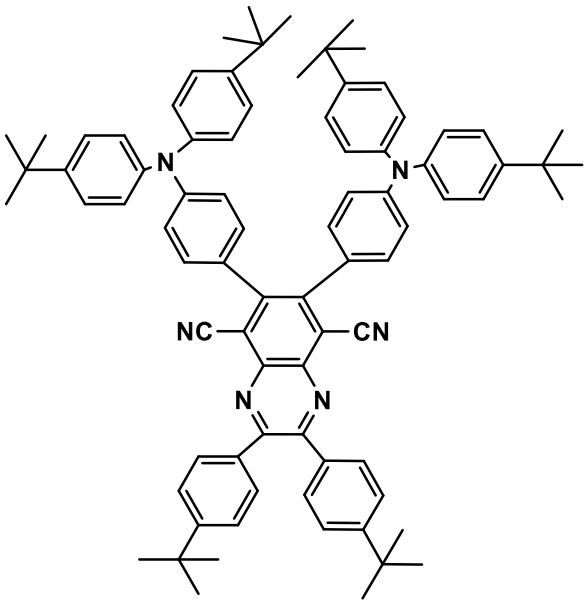

tBuTPA-CNQx

Fig. 4. Structure of ***t*BuTPA-CNQx** [26]

A key development in molecular design was achieved by the multiple resonance (MR) effect, a method that effectively facilitates the HOMO-LUMO separation even within a rigid, polycyclic aromatic skeleton, forming a small energy gap without utilizing the flexible D-A linkages to form TADF emitters that simultaneously show high efficiency, narrowband emission (full width at half maximum (FWHM) =28 nm), and exceptional color purity for deep blue light [21,23].

Despite remarkable progress, multiple drawbacks persist, such as efficiency decrease at high brightness, poor blue emitter stability, and synthetic complexity, which have limited their large-scale application [21].

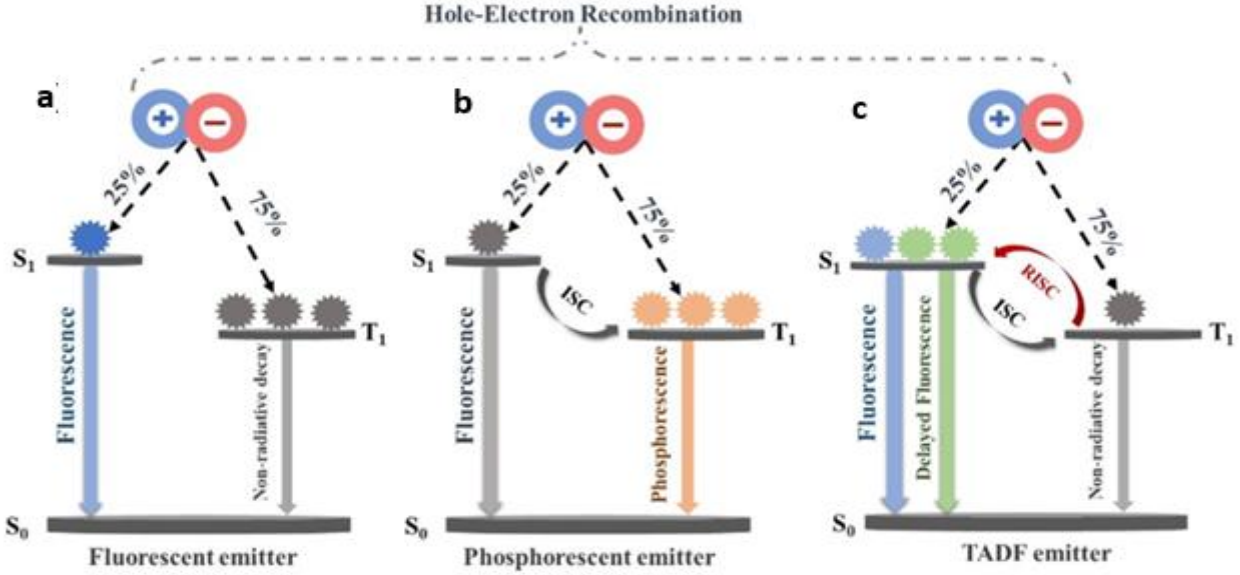

Fig. 5. Emission mechanism of fluorescent (a), phosphorescent(b), and TADF(c) emitter [6].

1.1.3. OLED fabrication methods

OLED fabrication fundamentally includes precise deposition and surface modification of several functional thin films [27]. The fabrication method significantly affects the device's performance, stability, and cost. Concerning the critical organic layers, the main deposition method is the vacuum thermal evaporation (VTE) (Figure 6).

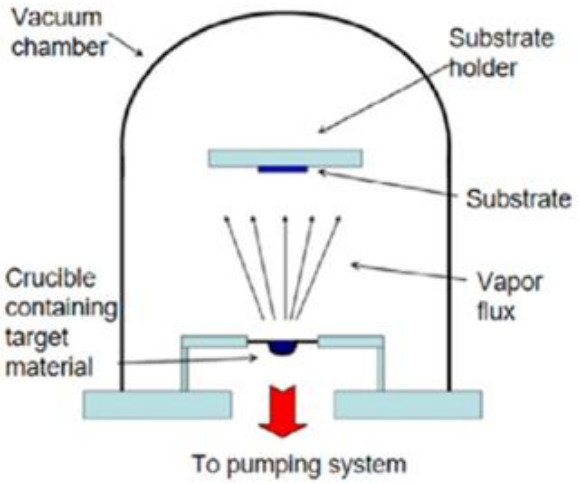

Fig. 6. Vacuum thermal evaporation mechanism [26].

In VTE fabrication, solid organic materials are positioned in evaporation sources and heated under vacuum, leading to sublimation. The formed vapor is directed upward and flows through a fine metal mask, forming patterned films on the substrate [27].

Since the vacuum techniques allow the fabrication of more sophisticated multi-layer device configurations, vacuum sublimation is the widely adopted method for manufacturing commercially viable OLEDs [2]. Additionally, solution-based deposition methods such as inkjet printing and blade-coating are developing as viable alternatives due to their scalability and compatibility with flexible and large-area substrates [28]. Among various solution-based techniques, the inkjet printing technique is distinguished as the most promising method, due to improved material utilization and reduction in device production costs [2, 27,30].

The major techniques for inkjet printing are classified into two types such as: "Continuous-Stream Inkjet (CIJ)" and "Drop-on-Demand (DoD)" (Figure 7) [27,29]. In both methods, the ink ejects through a small orifice (commonly called as a nozzle). In CIJ, as the name suggests, inkjet provides a continuous stream of ink droplets that are distinctly charged through the digital printing signals. The charged droplets are redirected by voltage plates into a gutter for recirculation and reutilization, while the neutral droplets are directly ejected onto the substrate. In the DoD fabrication method, as depicted in Figure 4, droplets are only ejected when needed (droplet-wise ejection). The ink is only introduced via the print head when a print dot is to be set. In front of the nozzle is an enclosure that is charged with ink. The ink is ejected via the nozzle by decreasing the volume of this enclosure. Although, a piezoelectric actuated printhead is used to achieve the required volume reduction of the ink enclosure [29].

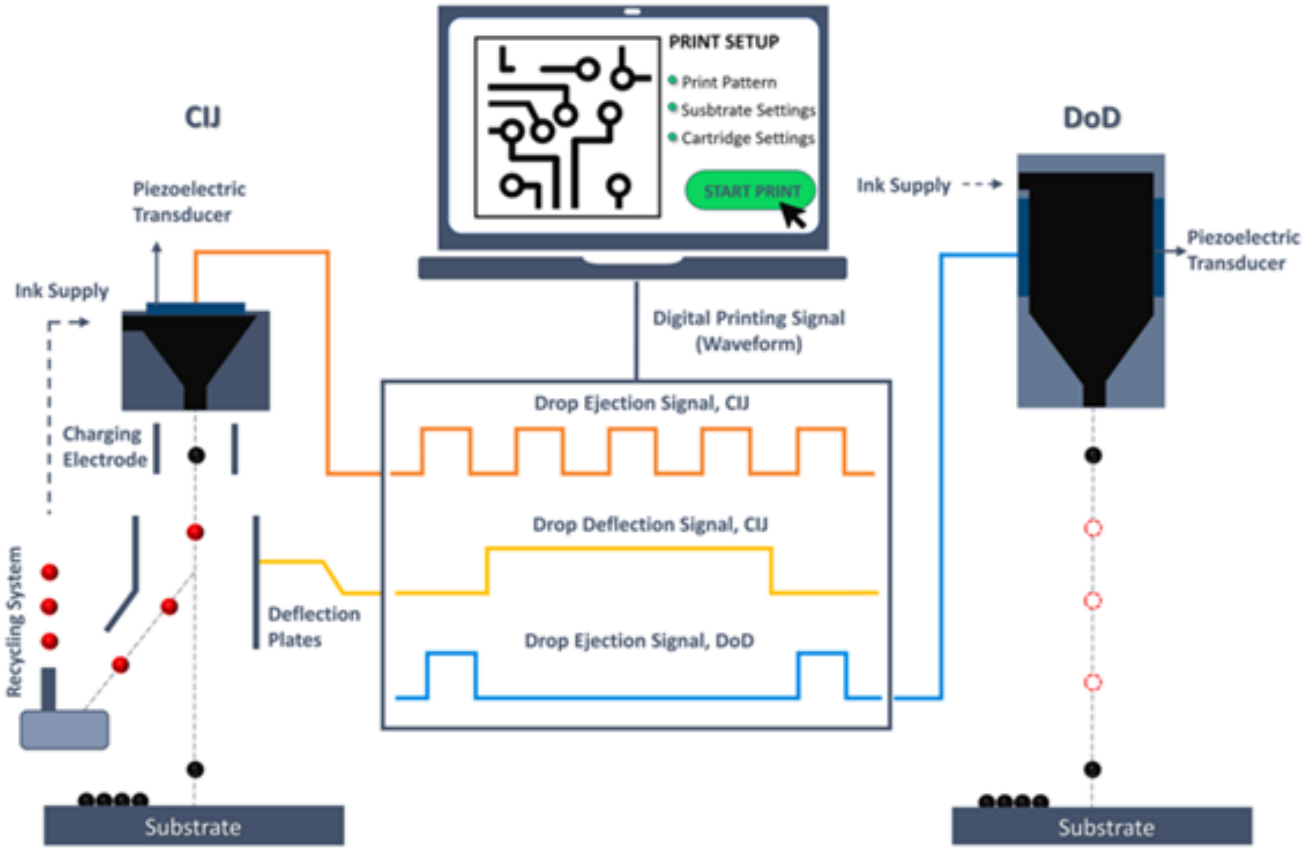

Fig. 7. Schematic illustration of CIJ and DoD inkjet printer [29].

However, the effectiveness and stability of solution-coated OLEDs remain low in comparison with their VTE counterpart. There are several factors for the weaker device efficiency of solution-processed OLEDs, which could be the inadvertently introduced impurities, non-optimized production conditions, non-uniformity of film structure, molecular aggregation, and dissolution of subjacent layers [30].

1.2. Deep-blue OLED emitters

The high-efficiency deep-blue luminescent materials are crucial in OLED applications, not only functioning as one of the three key colors, but also serving as host materials for the production of other monochromatic and white light. For commercial devices with adequate lifetimes and efficiency, deep-blue emissions with considerably higher efficiency and operation time are essential prerequisites. Scientists have generally accepted that an extremely deep-blue emitter can have a key role in developing an outstanding color gamut, which refers to the color produced by mixing two or more color lights to form a target color [31]. Additionally, it has been consistently confirmed that deep-blue emission has a key role in producing a high color rendering index (CRI) which is a significant indicator of light quality for utilization in art galleries and exhibition centers, as it can reflect the true color of paintings and artwork precisely under artificial light. Designing high-performance, low roll-off, and low cost deep-blue materials is still a challenge due to the inherent wide bandgap of deep-blue emissive materials leading to non-uniform carrier injection and transport in OLEDs [32].

Recent studies [33-36] have investigated the novel mechanisms underlying deep-blue fluorescent OLED materials, achieving noteworthy developments via the implementation of the hot exciton approach, which has led to significant innovations in device efficiency and stability, enabling promising insights for the further progress of OLED technology.

In 2022, Zeng et al. [36] presented three efficient deep-blue OLED fluorescent emitters named as **TTT-TPA-R** (R = H, OMe, tBu) (Figure 8) employing tris(trazolo)triazine as an acceptor and triphenylamine derivatives as a donor fragment by the route of "hot exciton". Excellent deep/pure blue emission in the region of 420–480 nm with 80–100% emission efficiency was obtained [36]. Exceptionally, these fluorescent emitters can harvest both singlet and triplet excitons through the RISC process from the high-lying triplet state to the singlet state. The solution-processable deep blue OLED exhibited the EQEmax of 10.5% [36].

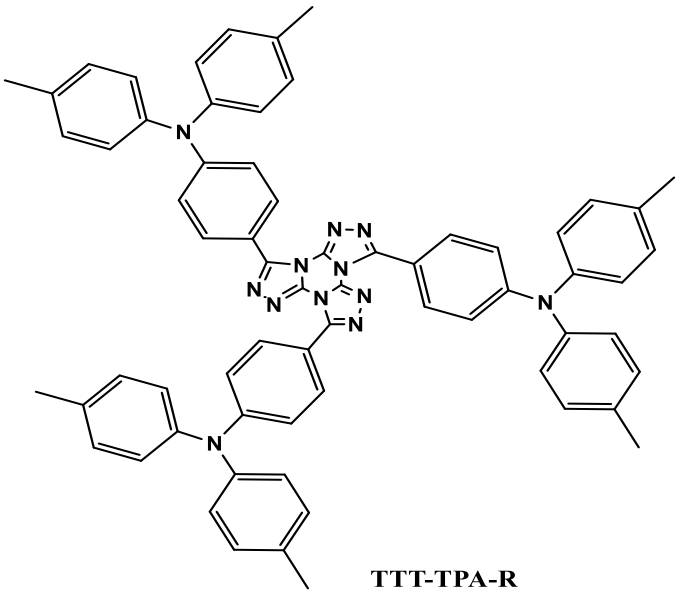

Fig. 8. Structure of **TTT-TPA-R (R = H, OMe, tBu)** [36]

Currently, a primary issue is the deficiency in high-performance blue phosphorescent materials that combine PLQY, high color purity, and enhanced stability. Against this background, Li et, al. [37] developed two new high-performance deep-blue tetradentate Pt(II) emitters (Figure 9) (Pt1 and Pt2) whose ligands consist of 1-(3,5-di-tert-butylphenyl)-9,9-dimethyl-1,9-dihydrofluoreno[2,3-d]imidazolium or 3-(3,5-di-tert-butylphenyl)-9,9-dimethyl-3,9 dihydrofluoreno[2,3-d]imidazolium carbene moiety (DMFI).

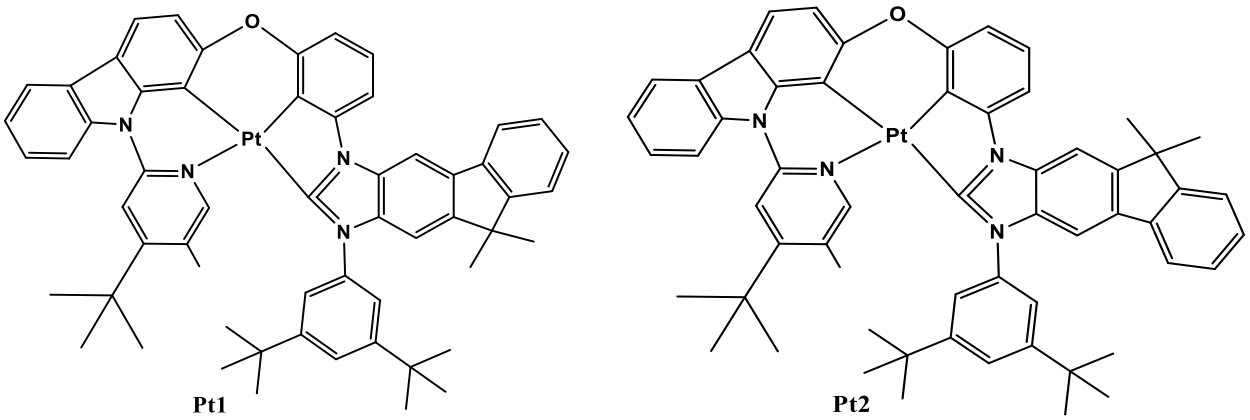

Fig. 9. Structure of **Pt1** and **Pt2** [37]

These Pt(II) emitters exhibit deep blue emission with a peak at 462–466 nm with excellent photophysical properties involving high PLQY of up to 90%, high EQE of 28.6% [37].

The deep-blue TADF emitters usually suffer from poor color purity and low efficiencies. To avoid these limitations, Mei et al. [38] introduced a series of deep blue TADF emitters (Figure 10). In this study, acridin-9(10H)-one (acridone, AD), characterized by orthogonal and highly rigid conformation, was used as an acceptor and carbazole as the donor to design **3,6-DDPhCz-AD** and **3,6-DDtBuPhCz-AD**, where the extended transition dipole moment, combined with high molecular rigidity, caused an outstanding radiative transition rate constant. **3,6-DDPhCz-AD** and **3,6-DDtBuPhCz-AD** showed EQE of 17.4% and 17.3% in doped OLEDs accordingly [38].

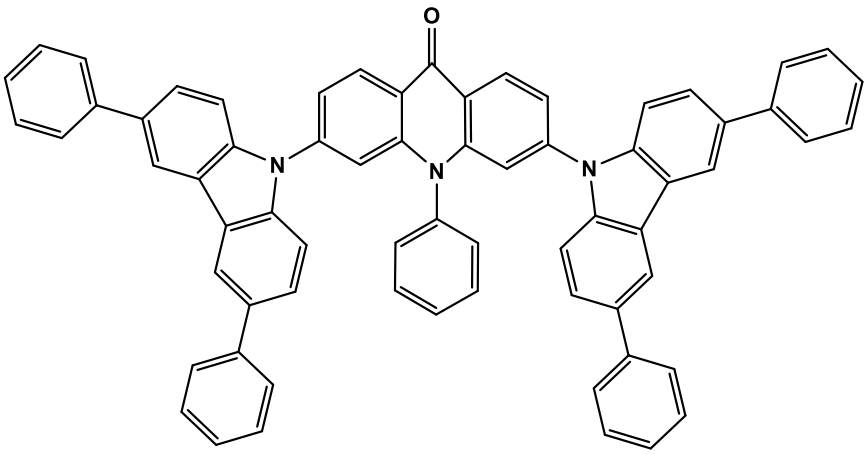

3,6-DDPhCz-AD (R1 &R2 =Ph)

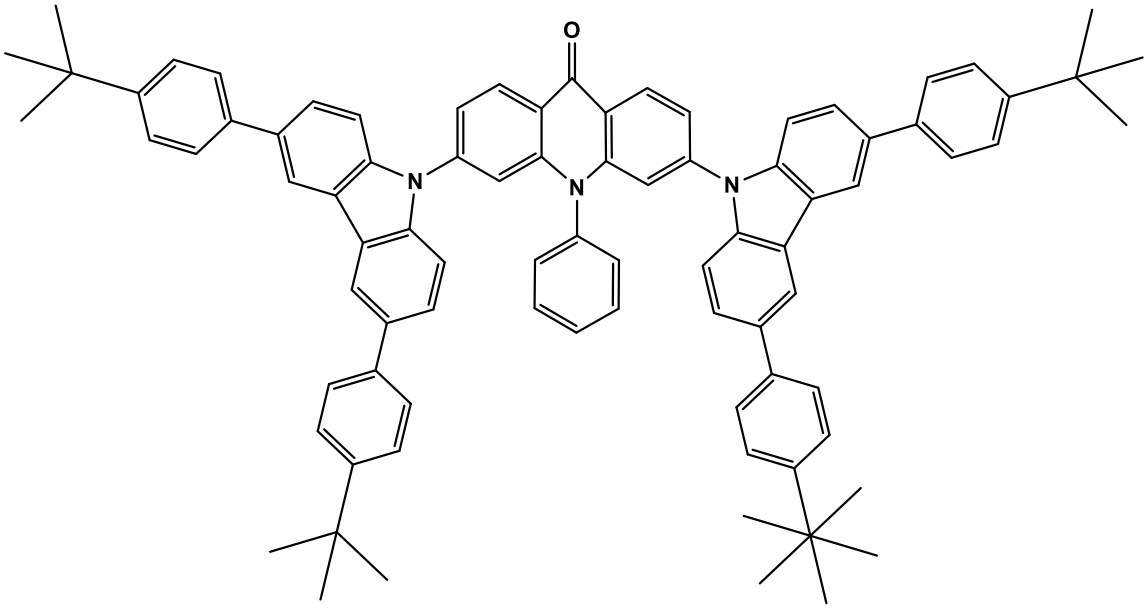

3,6-DDtBuPhCz-AD (R1 & R2 =tBuPh)

Fig. 10. Structure of **3,6-DDPhCz-AD** and **3,6-DDtBuPhCz-AD** [38]

1.3. Luminescent materials

1.3.1. Carbazole-based compounds

Carbazole is a multifunctional and promising heterocyclic building block extensively used in the organic materials due to its enhanced properties and applications across various fields, involving organic electronics [39]. In the field of OLEDs, carbazole has played a key role in their development, due to its characteristic properties such as low ionization potential, high hole mobility, high triplet energy, and blue/violet fluorescence, thus enabling its utilization in OLEDs. Its chemical and structural adaptability facilitates precise optimization of optoelectronic properties, involving superior PLQYs, high electrochemical and thermal stability [39-41].

Carbazole consists of an aromatic structure with significant electron delocalization. In the compound structure, the presence of pyrrole enhances the carbazole's electron-rich nature, and the hole transport property provided by its aromatic nature. The nitrogen in the pyrrole ring allows easy functionalization of carbazoles, designing various materials with versatile applications [41]. They can be utilized as common emitting materials, host materials for phosphorescence OLEDs, and TADF emitters [39-41]. Carbazoles serve as emission layers to enhance fluorescence quantum yields.

In 2025, Guo et al. [42] introduced deep-blue fluorescent emitter (Figure 11) 3,3'-(6-(4-(9H -carbazol-9-yl)phenyl)-1,3,5-triazine-2,4-diyl)bis(9-phenyl-9H -carbazole) (**2PhCzTRZ-Cz**).The non-doped OLEDs systems utilizing **2PhCzTRZ-Cz** as emission layer exhibited the EQE of 3.76-5.68% [42]. The **2PhCzTRZ-Cz** showed high thermal stability with decomposition temperature of 543 °C [42]. Furthermore, glass transition temperature of **2PhCzTRZ-Cz** was determined to be 180 °C [42].

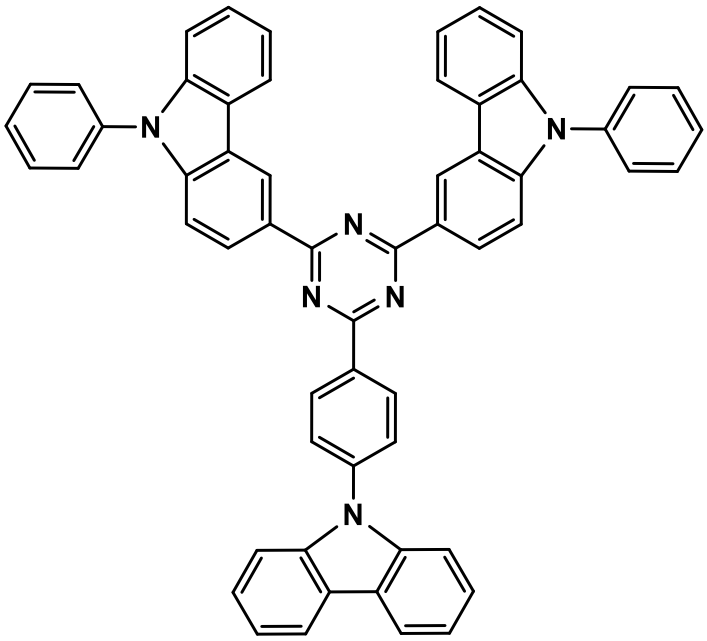

2PhCzTRZ-Cz

Fig. 11. Structure of **2PhCzTRZ-Cz** [42]

1.3.2. Fluorene and spirobifluorene-based compounds

Fluorene, defined by its rigid planar biphenyl configuration, has a key role in improving OLED technologies. Its enhanced photothermal stability and wide bandgap energy make it an exceptional compound within organic emitters, predominantly for blue light emission, which is a crucial component to obtain full-color OLED displays [43,44]. The molecular configuration of fluorene has a limited reactive site characteristic, which enables chemical modifications. This architectural tunability has enabled fluorene and its derivatives to exhibit fluorescence quantum efficiencies of 60% and 80% in solid state, thus making it a vital component of high-performance organic light emitting materials [45].

In 2025, Sun et al. [43] introduced a novel efficient near-ultraviolet emitter, namely 4-(7-(4-(4,5-diphenyl-4H-1,2,4-triazol-3-yl)phenyl)-9,9-dipropyl-9H-fluoren-2-yl)-N,N-diphenylaniline (**DTDPFDA**) (Figure 12) derived from the fluorene material. This compound exhibits deep-blue emission with an EQE of 5.7%. The material has a high decomposition temperature of 452 °C and a high glass transition temperature of 133 °C, showing its high thermal stability [43].

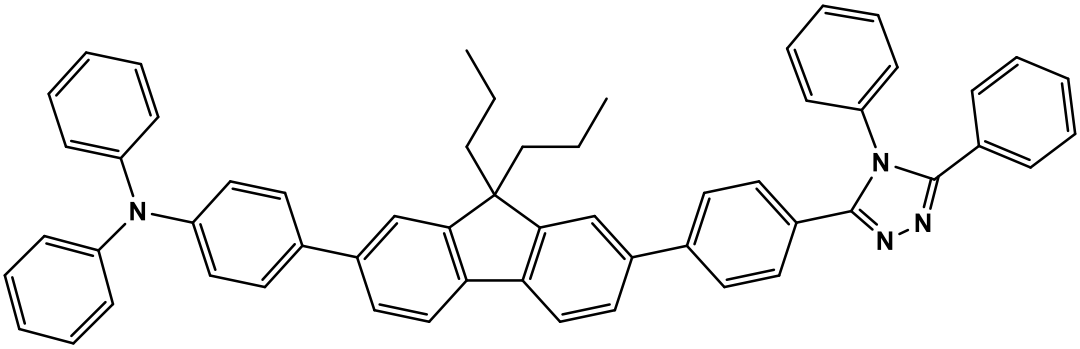

DTDPFDA

Fig. 12. Structure of **DTDPFDA** [43]

Spirobifluorene (SBF) (Figure 13) has been widely studied due to its rigid, non-planar framework that efficiently suppresses π-π stacking interactions and promotes the development of amorphous thin films with reduced crystallinity. Its orthogonal fluorene structure diminishes the electronic coupling between two units, thus sustaining unique optical properties. Furthermore, SBF shows outstanding electrochemical stability, as evidenced by its reversible oxidation and reduction features, which are essential to achieve reliable electronic performance. SBF-based materials also exhibit high solubility and suitability with diverse thin-film fabrication methods [46-49].

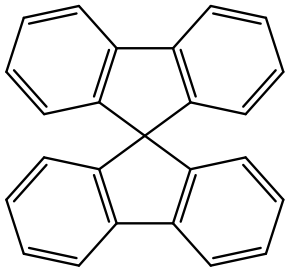

SBF

Fig. 13. Structure of **SBF** [47]

In 2025, Sun et al. [50] synthesized new hot exciton emitter designed on SBF core fragment. The material namely, **TPA-SBF-OXZ** (Figure 14) exhibit a blue emission at 468 nm, with an EQE of 10.2%, having PLQY of 70.7%. The **TPA-SBF-OXZ** showed excellent thermal stability with a decomposition temperature of 480 °C, and a glass-transition temperature of 162 °C. These values demonstrate the compound's high morphological stability in films [50].

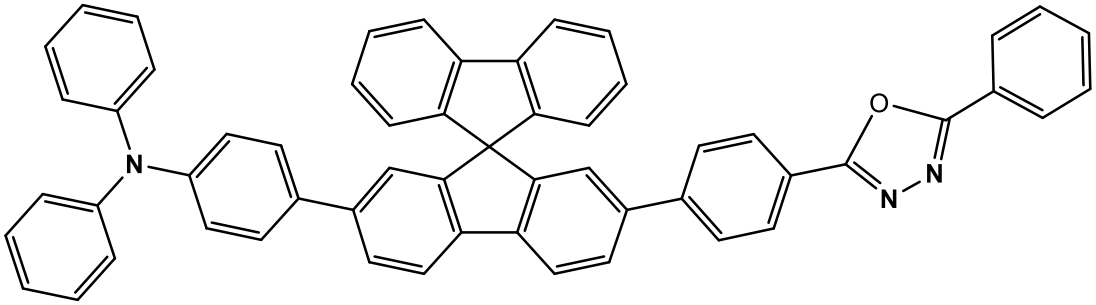

TPA-SBF-OXZ

Fig. 14. Structure of **TPA-SBF-OXZ** [50]

1.3.3. Dibenzofuran-based compounds

Dibenzofuran (DBF) (Figure 15) is characterized by the structure containing two benzene rings bridged by an electronegative oxygen heteroatom. The material demonstrates planar rigidity, while the carbon-oxygen bond's stretching motion leads to localized flexibility. This distinctive structural property promotes high molecular fluorescence efficiency without reducing solubility, resulting in a promising compound for solution-processable fluorescent materials [51]. Furthermore, dibenzofuran, an oxygen-bearing fused aromatic ring architecture, enables a highly stable bond structure, promoting high electrical and thermal stability [52].

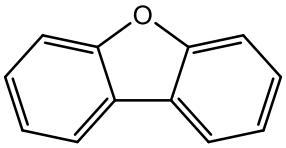

DBF

Fig. 15. Structure of **DBF** [53]

In 2025, Beresneviciute et al. [53] introduced two new carabazole and dibenzofuran-based emitting materials 3-[N,N-di(9-ethylcarbazol-9-yl)amino]-2-methoxydibenzofuran (**BeCzMFI**) and 3-[N,N-di(9-butylcarbazol-9-yl)amino]-2-methoxydibenzofuran (**BbCzMFI**) (Figure 16). These materials exhibit blue emission with EQEs of up to 10.4%, having PLQYs of 16.8% and 14.7%, respectively [53]. Both materials demonstrated high thermal stability with the decomposition temperatures of 360 °C and 411 °C, and they were obtained as fully amorphous compounds with glass transition temperatures of 132 °C and 100 °C for **BeCzMFI** and **BbCzMFI** in the same order [53].

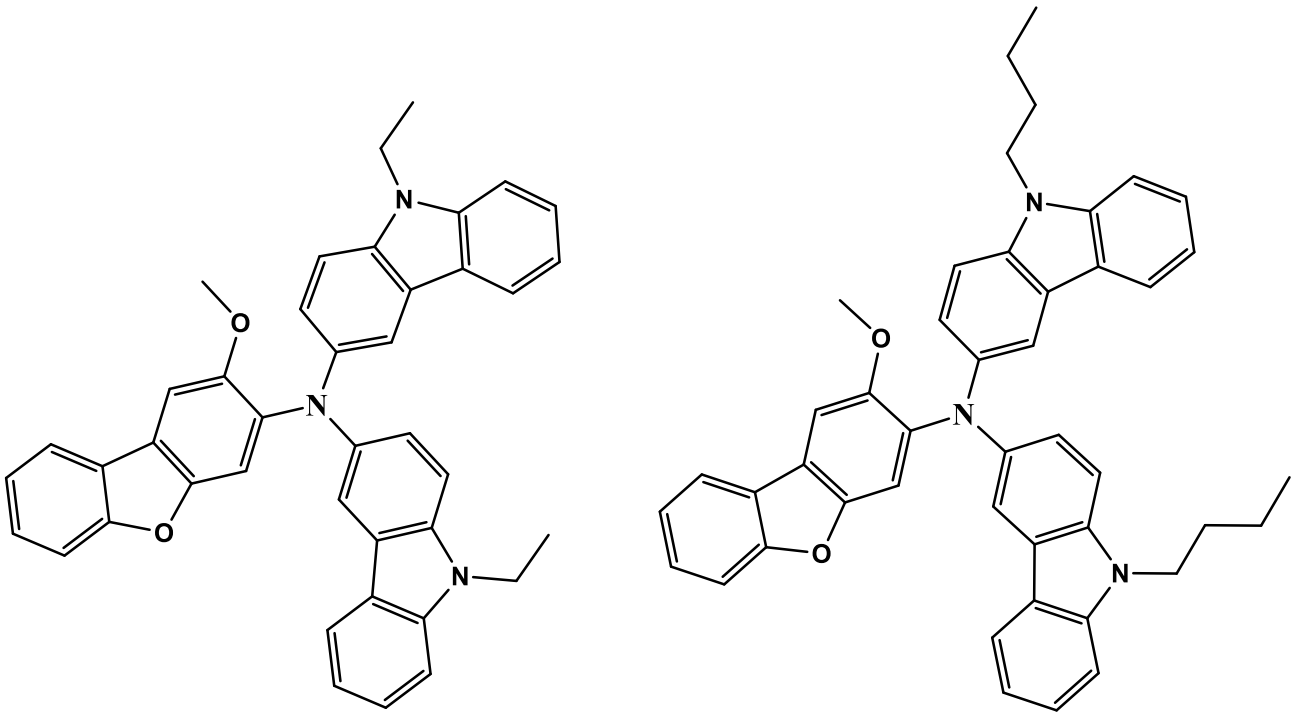

Fig. 16. Structure of **BeCzMFI** and **BbCzMFI** [53]

1.3.4. Thiophene-based compounds

Thiophene is a widely recognized, electron-rich, five-membered non-benzenoid aromatic hydrocarbon which consists of sulfur as a heteroatom [54]. Its popularity as a building block for organic materials is attributed to its high stability, efficient π-conjugation, and promising structural modification potential [54]. Thiophene presence not only promotes the charge transfer (CT) effect but also retains the locally excited (LE) component, inducing red-shifted emission peaks with high PLQY values [55].

In 2024, Ganczarczyk et al. [56]. synthesized two fluorene and thiophene-based emitters (Figure 17), namely 4,7-.bis(9,9-dihexyl-7-(thiophen-2-yl)-9H-fluoren-2-yl)benzo-[c][1,2,5]thiadiazole (**Th-FBTD**), 4,7-bis(7-([2,20-bithiophen]-5-yl)-9,9-dihexyl-9H-fluoren-2 yl)benzo[c][1,2,5]thiadiazole (**2ThFBTD**) emitting in green region at 540 nm, displaying high PLQY in solution (up to 95%) and in the solid state (up to 97%), and EQE of 3.5% (**Th-FBTD**) and 2.8% (**2ThFBTD**). Additionally, melting transition temperatures of Th-FBTD and 2ThFBTD was determined to be 114 °C and 216 °C, whereas the decomposition temperature of 425 °C and 442 °C were observed, revealing excellent thermal stability [56].

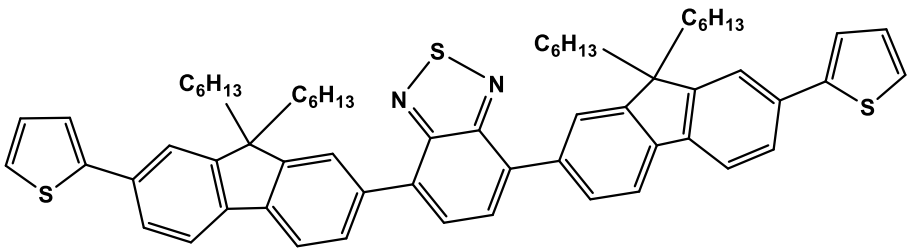

Th-FBTD

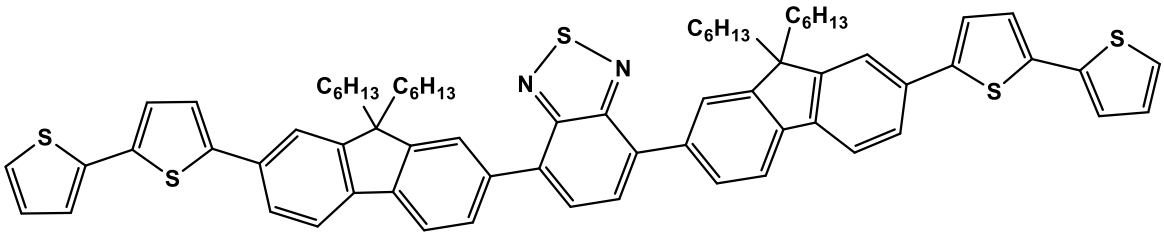

2Th-FBTD

Fig. 17. Structure of compounds **Th-FBTD** and **2ThFBTD** [56]

1.4. Literature summary

OLEDs are available in a broader range of forms than classical LEDs. They can be fabricated into flexible, transparent, and bendable panels, enabling advanced lighting designs and applications that are not viable with standard LEDs. Furthermore, OLEDs are consistent with global tendencies regarding energy conservation, emission reduction, and sustainable development, allowing them to be widely adopted for indoor, automotive, and medical lighting applications. OLED technology, with its key properties such as self-emissive nature, excellent color reproduction, wide viewing angles, potential for flexible design, and short response time, has emerged as the preferred choice for high-end smartphones, TVs, and wearable devices [57]. However, the low efficiency and stability of OLED devices remain as key limitations [5]. These drawbacks can be minimized by the production of advanced electroactive materials. Traditional techniques to synthesize electroactive materials suffer from low reaction yields, longer reaction times, hazardous material usage, high cost, and large amounts of reactants usage. It is vital to synthesize electroactive materials with low production costs, high efficiency, and operational stability. As evidenced by the literature review, carbazole, fluorene, spirobifluorene, dibenzofuran, and thiophene-based compounds exhibit enhanced characteristics such as low ionization potential, high thermal morphological stability, efficient π-conjugation, rigid, non-planar framework, promising structural modification potential and thus can be used to develop new electroactive materials. These distinctive properties promote high emission efficiency and stability.

2. Research part

2.1. Experimental Section

2.1.1. Instrumentation

Nuclear Magnetic Resonance (NMR)
Proton magnetic resonance spectra (1H NMR) were recorded on a Bruker Avance III (400 MHz) spectrometer. The spectral scale is graduated in parts per million (ppm). Tetramethylsilane (TMS) was used as an internal standard. Spectral analysis was performed in deuterated chloroform (CDCl3), tetrahydrofuran (THF), and dimethyl sulfoxide (DMSO) solutions.

Infrared spectroscopy (IR)
The IR spectra were recorded utilizing Perkin Elmer Spectrum GX II in KBr pellets. The infrared spectra are a plot of measured infrared intensities against frequencies.

Mass spectrometry (MS)
The mass spectra of the synthesized compounds were recorded on a Waters SQ Detector 2 mass spectrometer (ionization with 20 eV electron beam)

Photoluminescence spectroscopy
PL-spectra of 10-5 M solutions of the compounds were obtained using FLS980 Fluorescence Spectrometer. The drop casting method was used to prepare the thin films of the samples from a 1 mg/ml solution in diverse solvents. Measurements were performed by dr. Oleksandr Bezvikonnyi.

Photoluminescence decay curve analysis
PicoQuant LDH-D-C-375 laser with the excitation wavelength of 374 nm was utilized to measure PL decay curves. Measurements were performed by dr. Oleksandr Bezvikonnyi.

Time-solved photoluminescence analysis
uF920H lamp, classified as μF, was a Xe microsecond flash lamp utilized for the time-solved PL measurements. Measurements were performed by dr. Oleksandr Bezvikonnyi.

Thermogravimetric Analysis (TGA)
Thermogravimetric analysis was performed on a TA Instruments Q50 apparatus under nitrogen at a heating rate of 20 °C/min. Measurements were performed by dr. Eigirdas Skuodis and dr. Asta Dabulienė.

Differential Scanning Calorimetry (DSC)
Thermal transformations of materials were studied using the DSC Q100 TA instrument, a differential scanning calorimeter. Heating and cooling rates were 10 °C/min. Measurements were performed by dr. Eigirdas Skuodis and dr. Asta Dabulienė.

Cyclic Voltammetry (CV)
CV measurements were carried out using an Autolab Type III potentiostat. A 0.5 M tetrabutylammonium perchlorate solution in dry dichloromethane was used at room temperature, with a scan rate of 50 mV/s. Potentials were measured using a three-electrode cell containing a silver reference electrode, a carbon working electrode, and a platinum auxiliary electrode. A standard ferrocene/ ferrocene+ (FC/FC+) redox system was used for calibration.

Fabrication and investigations of OLEDs

The Avantes AvaSpec-2048XL spectrometer was utilized to record electroluminescence spectra. Kurt J. Lesker equipment built in the MBRAUN EcoVap4G glove box was employed for fabrication of OLEDs. Organic and metal OLED layers were fabricated by thermal vacuum evaporation on clean indium tin oxide (ITO) coated glass. Density-voltage and luminance-voltage measurements were performed by employing PH100-Si-HA-D0 photodiode, Keithley 6517B electrometer, Keithley 2400C sourcemeter, and 11S-LINK monitor. All investigations were performed in air at room temperature. Device fabrication and characterization was performed by dr. Oleksandr Bezvikonnyi.

2.1.2 Materials and Methods

2,7-Dibromo-9,9-dimethyl-9H-fluorene($C_{15}H_{12}Br_2$), 2,7-dibromo-9,9'-spirobifluorene ($C_{25}H_{14}Br_2$), (9-phenyl-9H-carbazol-3-yl)-boronic acid ($C_{18}H_{14}BNO_2$) (materials sourced from Fluorochem), (6-phenyldibenzo[b,d]furan-4-yl)boronic acid ($C_{18}H_{13}BO_3$) (material sourced from BLD Pharm), 5,5''-dibromo-2,2':5',2''-terthiophene($C_{12}H_6Br_2S_3$) (material sourced from BLD Pharm), (9-phenyl-9H-carbazol-2-yl)boronic acid($C_{18}H_{14}BNO_2$) (material sourced from Fluorochem), (9,9'-spirobi[fluoren]-2-yl)boronic acid($C_{25}H_{17}BO_2$) (material sourced from BLD Pharm), bis(triphenylphosphine) palladium(II) dichloride ($[(C_6H_5)_3P]_2PdCl_2$) (material sourced from Sigma-Aldrich), dimethyl sulfoxide (C_2H_6OS) (materials sourced from Realchem), dichloromethane (CH_2Cl_2) (materials sourced from Eurochemical), ethyl acetate ($C_4H_8O_2$) (materials sourced from Eurochemical), nefras 80/120, toluene ($C_6H_5CH_3$) (materials sourced from Eurochemical), dimethylformamide ($HCON(CH_3)_2$) , hexane (C_6H_{14}), acetone (C_3H_6O), tetrahydrofuran (C_4H_8O), sodium sulfate (Na_2SO_4) (materials sourced from Eurochemical), potassium carbonate (K_2CO_3) (materials sourced from Realchem), silica gel 60 Angstrom (material sourced from Supelco.)

6,6'-(9,9-Dimethyl-9H-fluorene-2,7-diyl)bis(4-phenyldibenzo[b,d]furan) (1).

2,7-Dibromo-9,9-dimethyl-9H-fluorene (0.2 g, 0.568 mmol), and (6-phenyldibenzo[b,d]furan-4-yl)boronic acid(0.3683 g, 1.278 mmol) were dissolved in dimethylformamide (DMF) (12 ml) separately and added to a Schlenk flask. The mixture was stirred under vacuum for 20 minutes, subsequently purged with argon gas to create an inert atmosphere. Bis(triphenylphosphine) palladium(II) dichloride (catalyst, 0.0079 g, 0.0113 mmol) was added to the reaction and then all the mixture was stirred for 15 minutes. 0.565 M potassium carbonate (0.1559 g, 1.13 mmol) solution was added to the reaction flask. The reaction mixture was stirred at 80 °C for 24 hours and then cooled to ambient temperature. Distilled water (150ml) was added to the reaction mixture, and the organic phase was extracted with dichloromethane (DCM) (3 x 150ml), organic phase was dried with sodium sulfate (30 g), followed by filtering and evaporating the DCM solvent. Organic matter was purified with silica gel column chromatography using a mixture of tetrahydrofuran:hexane 1:2 ratio as eluent. Data regarding column chromatography are given in Table 1. The yield of white solid was 80% (0.308 g). $C_{51}H_{34}O_2$. MW=678.81 g/mol.

^{1}H NMR (400 MHz, THF) δ 1.57 – 1.62 (s, 6H), 7.34 – 7.44 (s, 2H), 7.44 – 7.56 (p, J = 7.5 Hz, 8H), 7.68 – 7.75 (d, J = 7.5 Hz, 2H), 7.76 – 7.82 (d, J = 7.6 Hz, 2H), 7.91 – 8.11 (m, 12H), 8.18 – 8.22 (s, 2H).

FT-IR (KBr, cm^{-1}): 3049 (Ar. C – H), 2921 (Alkane C – H), 2337 (Alkyne C = C), 1599 (Ar. C – C), 1408 (Alkane C – H), 1180 (Ether C – O), 903 (Alkene C – H).

MS: m/z 678 $[(M+H)^+]$

Table 1. Column Chromatography details

Product	**Static Phase Height**	**Solvent**	**Solvent Ratio**
1	12 cm	THF : Hexane	1:2
2	12 cm (1st Purification)	Hexane : Acetone	50 : 1
	5 cm (2nd Purification)	THF : Hexane	1:2
3	12 cm	THF : Hexane	1:7
4	12 cm	THF : Hexane	1:7

2,7-Bis(6-phenyldibenzo[b,d]furan-4-yl)-9,9'-spirobi[fluorene] (2).

2,7-Dibromo-9,9'-spirobifluorene (0.4 g, 0.844 mmol) and (6-phenyldibenzo[b,d]furan-4-yl)boronic acid (0.5468 g, 1.898 mmol) were dissolved in DMF (12 ml) separately and added to a Schlenk flask. The mixture was stirred under vacuum for 20 minutes, subsequently purged with argon gas to create inert atmosphere. Bis(triphenylphosphine) palladium(II) dichloride (catalyst, 0.0118 g, 0.0168 mmol) was added to reaction and then all the mixture was stirred for 15 minutes. 0.565 M potassium carbonate (0.3118 g, 2.256 mmol) solution was added to the reaction flask. The reaction mixture was stirred at 80 °C for 24 hour and then cooled to ambient temperature. 150 ml distilled water was added to the reaction mixture and the organic phase was extracted with DCM (3 x 150ml), organic phase dried with sodium sulfate (30 g) followed by filtering and evaporating of DCM solvent. Two silica gel column chromatography performed for organic matter purification with the mixture of acetone:hexane (1:50) as an eluent and tetrahydrofuran:hexane (1:2) for second column chromatography. The yield of white solid was 61% (0.412 g). $C_{61}H_{36}O_2$. MW=800.94 g/mol.

^{1}H NMR (400 MHz, $CDCl_3$) δ 8.23 (d, J = 7.8 Hz, 2H), 7.96 (d, J = 8.0 Hz, 2H), 7.92 (d, J = 7.5 Hz, 4H), 7.85 (d, J = 7.6 Hz, 2H), 7.79 (d, J = 6.0 Hz, 4H), 7.58 (d, J = 7.4 Hz, 2H), 7.50 (t, J = 7.2 Hz, 4H), 7.43 – 7.33 (m, 4H), 7.30 (t, J = 7.7 Hz, 4H), 7.22 (d, J = 7.5 Hz, 2H), 7.07 – 6.99 (m,4H), 6.81 (d, J = 7.4 Hz, 2H).

^{13}C NMR (101 MHz, $CDCl_3$) δ 14; 22; 25; 31; 34; 68; 77; 119; 120; 123; 124.4; 125; 126; 127; 128; 129; 136; 141; 148; 149; 153.

FT-IR (KBr, cm^{-1}): 3048 (Ar. C – H), 2948 (Alkane C – H), 2357 (Alkyne C = C), 1412 (Ar. C – C), 1185 (Ether C – O), 829 (Alkene C – H). MS: m/z 799 $[(M+H)^+]$

3,3'-(9,9-Dimethyl-9H-fluorene-2,7-diyl)-bis(9-phenyl-9H-carbazole) (3).

2,7-Dibromo-9,9-dimethyl-9H-fluorene (0.4 g, 1.136 mmol) and (9-phenyl-9H-carbazol-3-yl)-boronic acid (0.734 g, 2.556 mmol) by the same procedure as target compound (**2**). The organic matter

was purified with silica gel column chromatography using mixture of tetrahydrofuran:hexane (1:7) as an eluent. The yield of white solid was 57% (0.435 g). C51H36N2. MW=676.84 g/mol.

^{1}H NMR (400 MHz, CDCl3) δ 8.13 – 8.00 (s, 2H), 7.92 – 7.83 (d, J = 7.7 Hz, 2H), 7.54 – 7.50 (s, 1H), 7.50 – 7.47 (s, 1H), 7.46 – 7.42 (s, 2H), 7.41 – 7.32 (t, J = 7.7 Hz, 4H), 7.31 – 7.26 (s, 3H), 7.19 – 7.14 (s, 2H), 7.14 – 7.11 (s, 4H), 7.10 – 7.06 (d, J = 4.0 Hz, 4H), 7.01 – 6.92 (dt, J = 8.0, 3.5 Hz, 2H), 1.37 – 1.28 (s, 6H).

^{13}C NMR (101 MHz, CDCl3) δ 154; 141; 140; 137; 134; 130; 126; 125; 124; 123; 121; 120; 118; 110; 47; 31; 27; 22; 14.

FT-IR (KBr, cm-1): 3060 (Ar. C – H), 2976 (Alkane C – H), 2358 (Alkyne C = C), 1596 (Ar. C – C), 1438 (Alkane C – H), 1179 (Amine C – N), 831 (Alkene C – H)

MS: m/z 676 [(M+H)+]

2,7-Bis(9-phenyl-9H-carbazol-3-yl)-9,9'-spirobi[fluorene] (4).

2,7-Dibromo-9,9’-spirobifluorene (0.4 g, 0.844 mmol) and (9-phenyl-9H-carbazol-3-yl)-boronic acid (0.545 g, 1.898 mmol) by the same procedure as the target compound (**2**). The organic matter was purified with silica gel column chromatography using a mixture of tetrahydrofuran:hexane (1:7) as an eluent. The yield of white solid was 67% (0.449 g). C61H38N2. MW=798.97 g/mol.

^{1}H NMR (400 MHz, CDCl3) δ 8.23 (s, 2H), 8.16 (d, J = 7.7 Hz, 2H), 8.02 (d, J = 7.9 Hz, 2H), 7.93 (t, J = 9.5 Hz, 2H), 7.80 (d, J = 7.9 Hz, 2H), 7.62 (t, J = 7.5 Hz, 4H), 7.56 (d, J = 8.4 Hz, 5H), 7.52 (s, 1H), 7.51 – 7.45 (m, 3H), 7.45 – 7.40 (m, 6H), 7.37 (d, J = 8.5 Hz, 2H), 7.33 – 7.26 (m, 3H), 7.20 (t, J = 7.5 Hz, 2H), 6.96 (d, J = 7.6 Hz, 2H).

^{13}C NMR (101 MHz, CDCl3) δ 149; 141; 140; 137; 133; 129; 128; 127; 126; 125; 124; 123; 122; 120; 118; 109.

FT-IR (KBr, cm-1): 3042 (Ar. C – H), 2360 (Alkyne C = C), 1596 (Ar. C – C), 1452 (Alkane C – H), 1230 (Amine C – N), 871 (Alkene C – H).

MS: m/z 798 [$(M+H)^{+}$]

2-(5''-Bromo-[2,2':5',2''-terthiophen]-5-yl)-9-phenyl-9H-carbazole (5).

5,5''-Dibromo-2,2':5',2''-terthiophene (0.2 g, 0.492 mmol), and (9-phenyl-9H-carbazol-2-yl)boronic acid (0.14 g, 0.492 mmol) were dissolved in dimethyl sulfoxide (DMSO) (20 ml) separately and added to a Schlenk flask. The mixture was stirred under vacuum for 20 minutes, subsequently purged with argon gas to create an inert atmosphere. Bis(triphenylphosphine) palladium (II) dichloride (catalyst, 0.014 g, 0.002 mmol) was added to the reaction and then the mixture was stirred for 15 minutes. 0.984 M potassium carbonate (0.2722 g, 1.97 mmol) solution was added to the reaction flask. The reaction mixture was stirred at 80 °C for 15 minutes and then cooled to ambient temperature. Distilled water (150ml) was added to the reaction mixture, and the organic phase was extracted with DCM (3 x 150ml), organic phase was dried with sodium sulfate (30 g), followed by filtering and evaporating the DCM solvent. Organic matter was purified with silica gel (20 cm height)

column chromatography using Nefras as eluent. The yield of the yellow solid was 29% (0.08 g). $C_{30}H_{18}BrNS_3$. MW=568.57 g/mol.

^{1}H NMR (400 MHz, CDCl3) δ 6.91 (d, J = 4.0 Hz, 1H), 6.98 (d, J = 3.8 Hz, 1H), 7.02 (d, J = 3.9 Hz, 1H), 7.08 (d, J = 3.4 Hz, 1H), 7.14 (d, J = 3.8 Hz, 1H), 7.25 (s, 1H), 7.31 (d, J = 7.4 Hz, 1H), 7.41 (d, J = 8.1 Hz, 2H), 7.49 – 7.55 (m, 2H), 7.57 (t, J = 4.7 Hz, 2H), 7.60 (s, 1H), 7.66 (t, J = 7.7 Hz, 2H), 8.12 (s, 1H), 8.14 (s, 1H).

^{13}C NMR (101 MHz, CDCl3) δ 189; 182; 160; 158; 150; 144; 141; 137; 136; 135; 134; 131; 130; 127; 126; 124; 123; 120; 118; 111; 109; 106; 99.

MS: m/z 568 [$(M+H)^+$]

5,5''-Bis(9-phenyl-9H-carbazol-2-yl)-2,2':5',2''-terthiophene (6).

The target compound (**6**) was synthesized throughout the reaction for the intermediate compound (**5**). The organic matter co-purified during chromatic purification of intermediate compound (**5**) and eluted from the column by using nefras:toluene (1:1) mixture as an eluent. The yield of the brown solid was 10 % (0.034 g). $C_{48}H_{30}N_2S_3$. MW=730.96 g/mol.

^{1}H NMR (400 MHz, CDCl3) δ 7.10 (s, 2H), 7.14 (d, J = 3.8 Hz, 2H), 7.30 (t, J = 7.0 Hz, 6H), 7.41 (d, J = 7.4 Hz, 4H), 7.48 – 7.62 (m, 9H), 7.66 (t, J = 7.6 Hz, 4H), 8.13 (d, J = 7.9 Hz, 3H).

^{13}C NMR (101 MHz, CDCl3) δ 210; 207; 196; 174; 158; 154; 147; 144; 141; 137; 136; 131; 130; 127; 126; 124; 120; 118; 109; 106; 94; 70; 60; 57; 30; 26.

MS: m/z 730 [$(M+H)^+$]

2-(5''-(9,9'-Spirobi[fluoren]-2-yl)-[2,2':5',2''-terthiophen]-5-yl)-9-phenyl-9H-carbazole (7).

2-(5''-Bromo-[2,2':5',2''-terthiophen]-5-yl)-9-phenyl-9H-carbazole (0.353 g, 0.621 mmol), and 9,9'-spirobi[fluoren]-2-ylboronic acid (0.447 g, 1.242 mmol) were dissolved in DMSO (20 ml) separately and added to a Schlenk flask. The mixture was stirred under vacuum for 20 minutes, subsequently purged with argon gas to create an inert atmosphere. Bis(triphenylphosphine) palladium (II) dichloride (catalyst, 0.0436 g, 0.062 mmol) was added to the reaction and then the mixture was stirred for 15 minutes. 1.66 M potassium carbonate (0.687 g, 4.97 mmol) solution was added to the reaction flask. The reaction mixture was stirred at 80 °C for 24 hours and then cooled to ambient temperature. Distilled water (150ml) was added to the reaction mixture, and the organic phase extracted with ethyl acetate (3 x 150ml), followed by filtering the ethyl acetate solvent, from which the target compound (**7**) was obtained as a solid deposited on the filter paper surface. The yield of the bronze solid was 45% (0.227 g). C55H33NS3. MW=804.06 g/mol.

^{1}H NMR (400 MHz, THF) δ 6.63 (d, J = 7.7 Hz, 1H), 6.72 (d, J = 7.6 Hz, 2H), 6.96 (s, 1H), 7.02 – 7.21 (m, 8H), 7.24 (s, 1H), 7.35 (t, J = 4.4 Hz, 6H), 7.53 (d, J = 7.3 Hz, 1H), 7.55 – 7.62 (m, 2H), 7.67 (dd, J = 6.4, 13.6 Hz, 5H), 7.93 (q, J = 7.9 Hz, 4H), 8.15 (t, J = 9.2 Hz, 2H).
^{13}C NMR (101 MHz, THF) δ 203; 197; 195; 185; 174; 168; 163; 158; 156; 149; 148; 144; 142; 141; 137; 135; 133; 131; 129; 127; 125; 124; 123; 120; 119; 117; 109; 106; 99; 87; 83; 77; 70; 56; 29; 27; 13.
A mass spectrum was not obtained.

2.2. Results and discussion

2.2.1. Synthesis and Thermal Properties

The synthesis of the derivatives of 2,7-dibromo-9,9-dimethyl-9H-fluorene and 2,7-dibromo-9,9'-spirobi[fluorene] is shown in Scheme 1, and the synthesis of the derivatives of 5,5''-dibromo-2,2':5',2''-terthiophene is shown in Scheme 2. For the synthesis of target compounds, Suzuki coupling reactions of 2,7-dibromo-9,9-dimethyl-9H-fluorene and 2,7-dibromo-9,9'-spirobi[fluorene] with (6-phenyldibenzo[b,d]furan-4-yl)boronic acid or (9-phenyl-9H-carbazol-3-yl)boronic acid were carried out in the presence of bis(triphenylphosphine) palladium(II) dichloride as a catalyst and potassium carbonate as a base. The reactions produced donor-π-donor (D-π-D) derivatives **1**, **2**, **3**, **4** in yields of 80%, 61%, 57%, and 67%, respectively.

The target compounds were purified by column chromatography. The structures of the synthesized compounds **1**, **2**, **3**, and **4** were confirmed by ^{1}H NMR and FT-IR spectroscopies, **2**, **3**, and **4** by ^{13}C NMR, and **1**, **3** by mass spectrometry. Target compounds **1**, **2**, **3,** and **4** were found to be soluble in only chloroform and tetrahydrofuran.

Additionally, for the synthesis of target compounds **6** and **7**, the Suzuki coupling reaction of 5,5''-dibromo-2,2':5',2''-terthiophene with (9-phenyl-9H-carbazol-2-yl)boronic acid was carried out, as shown in Scheme 2. The resulting intermediate compound (**5**) was subsequently coupled with (9,9'-spirobi[fluoren]-2-yl)boronic acid in the presence of bis(triphenylphosphine) palladium(II) dichloride as a catalyst and potassium carbonate as a base.

The target terthiophene-based compounds **6** and **7** were obtained with the yields of 10 and 45 %, respectively. The target compound (**6**) was purified by column chromatography by using nefras:toluene (1:1) mixture as an eluent, whereas target compound (**7**) was isolated by filtration and washed with hexane. The structures of the synthesized compounds **5**, **6,** and **7** were confirmed by ^{1}H, ^{13}C NMR, and **5**, **6** by mass spectrometry. Target compounds **6** and **7** were found to be moderately soluble in organic solvents.

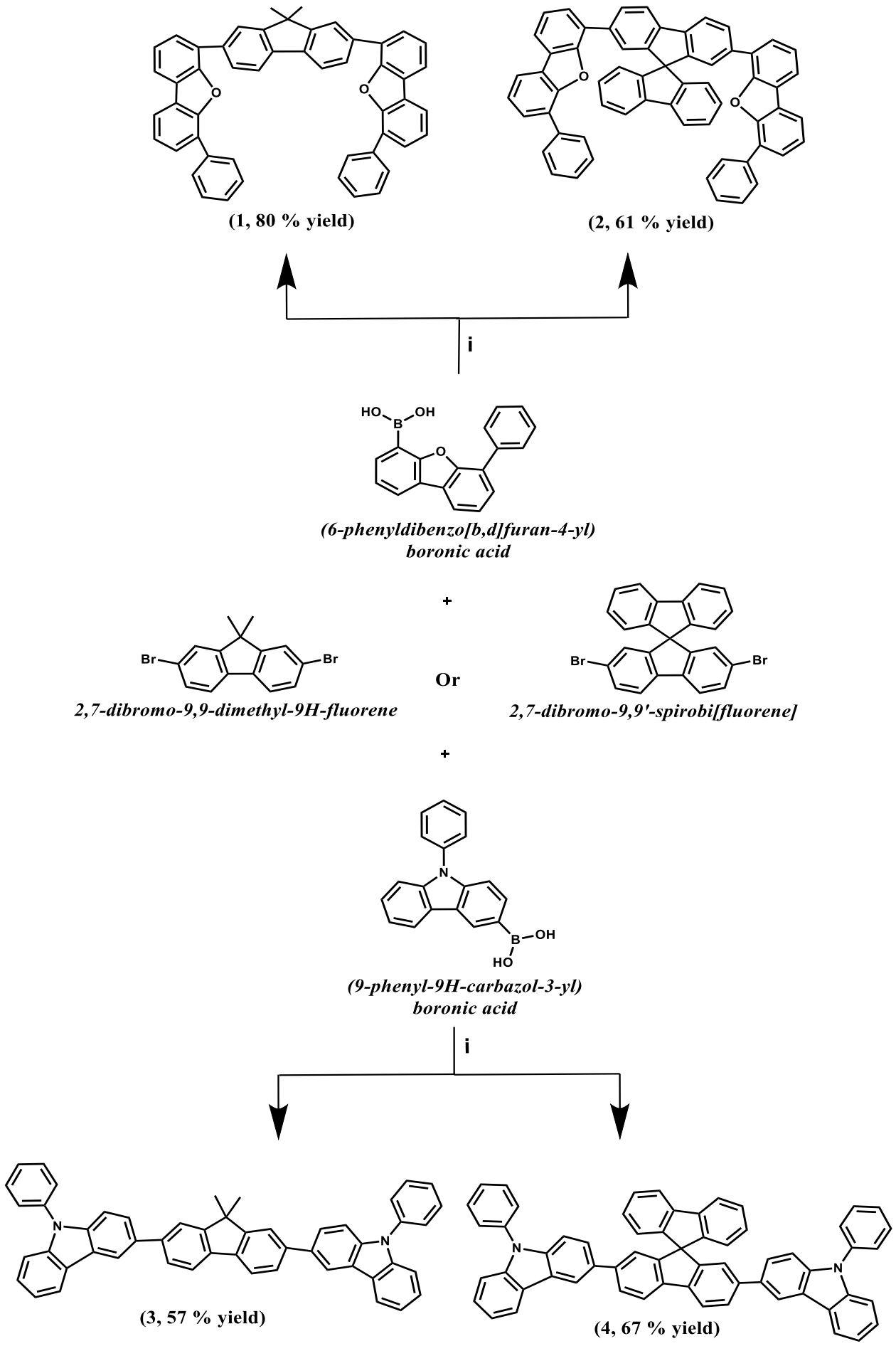

Scheme 1. Synthesis of target compound **1**,**2**,**3** and **4**: i) K_2CO_3,$[(C_6H_5)_3P]_2PdCl_2$,DMF,80°C,24 h.

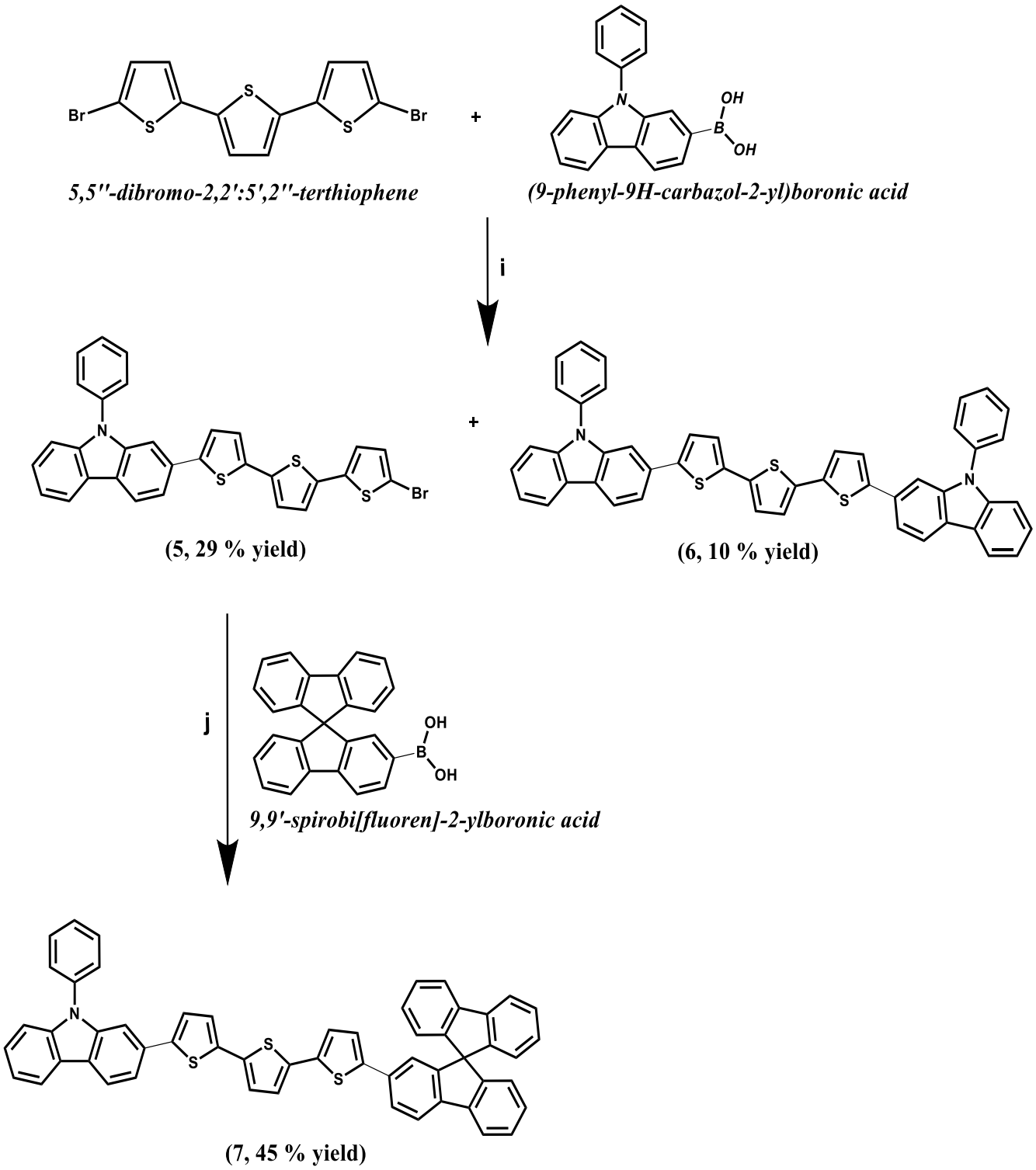

Scheme 2. Synthesis of intermediate compound **5** and target compounds **6, 7:** i) K_2CO_3, $[(C_6H_5)_3P]_2PdCl_2$, DMSO,80°C,15 min; j) K_2CO_3, $[(C_6H_5)_3P]_2PdCl_2$, DMSO,80°C,24 h.

Thermogravimetric analysis was used to estimate the thermal stability and decomposition temperature of compounds. The compounds are characterized by high thermal stability and are suitable for layer formation by vacuum evaporation [58] confirmed by TGA (Figure 18). Attributable to the presence of the spirobifluorene moiety, which contributes to molecular rigidity and its high molecular mass**,** compound **7** exhibited superior thermal destruction temperature. The thermal behavior investigations of the synthesized compounds clearly showed that due to high thermal

stability and adequate characteristics, all target compounds (**1-4**,**6**,**7**) are suitable for vacuum deposition in OLED fabrication.

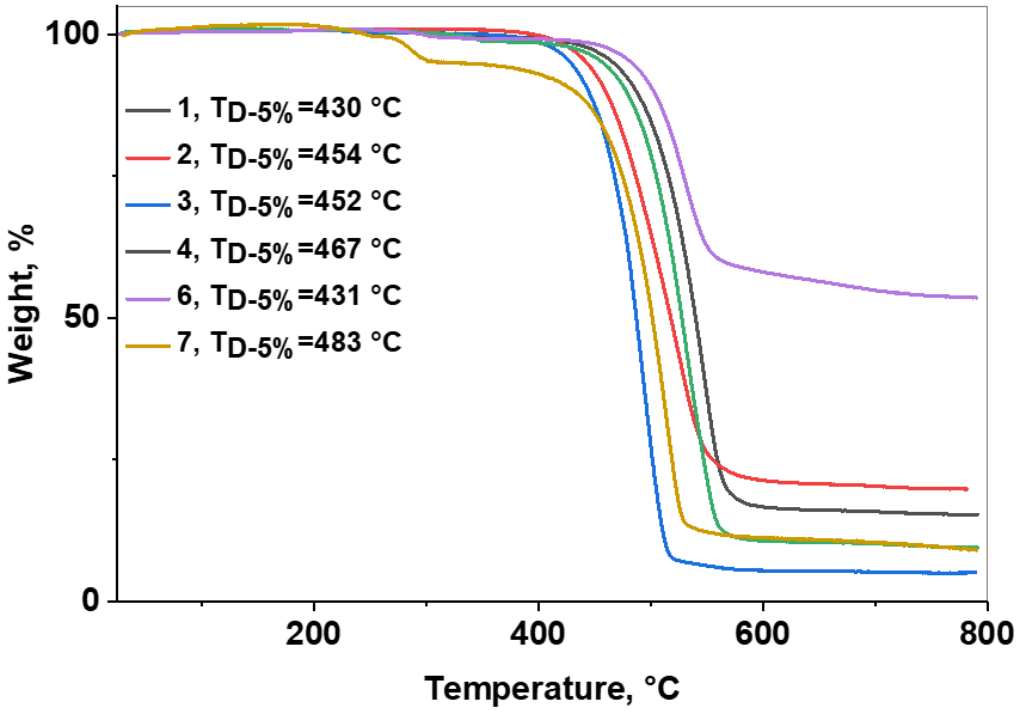

Fig. 18. TGA curves of compounds **1-4**,**6**,**7**.

Differential scanning calorimetry (DSC) was used to estimate the morphological transitions in the compounds **1-4**, **6**, and **7**. The detection of melting peaks during the initial scan reveals that all compounds were obtained as crystalline material (Figure 19-20). During the second heating scan of compound **3**, no observation of melting or crystallization transitions suggests outstanding thermal stability in contrast with other compounds. Compound **2** exhibits higher melting (365 °C) point compared to its carbazole-substituted analog that can be associated with more symmetric and simpler structure of phenyl group relative to bulkier carbazole moiety. Dimethylfluorene core derivatives **1** and **3** exhibit lower melting points 245 °C and 218 °C, respectively, compared to spirobifluorene core derivatives **2**(365 °C) and **4**(347 °C), can be ascribed to higher packing efficiency and rigidity of spirobifluorene core molecule, whereas dimethyl-substituted fluorene core demonstrates more dynamic molecular structure. Furthermore, compounds **1** and **3** demonstrated remarkably higher glass transition temperatures 128 °C and 140 °C, respectively, indicating superior thermal stability compared to their previously published host pyrene-substituted fluorene that exhibited glass transition at 76 °C [59].

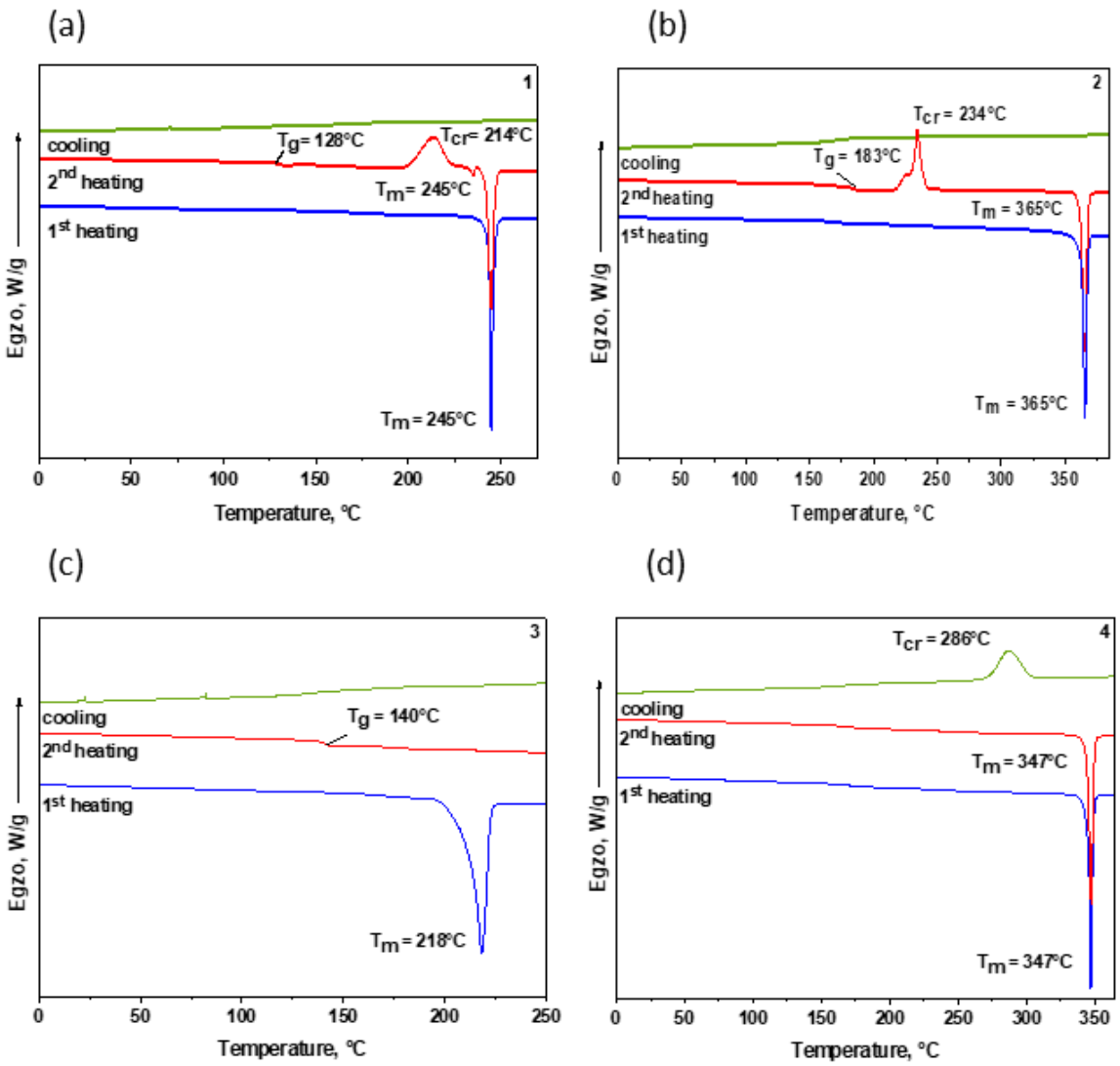

Fig. 19. DSC curves of compounds **1**(a), **2**(b), **3**(c), **4**(d).

Compound **7** exhibits higher melting point (289 °C) compared to its carbazol-substituted analog that can be associated with higher molecular rigidity and complex structure of spirobifluorene functional group relative to less bulky carbazole moiety (Fig. 20). During the second heating scan of compound **7**, no observation of melting or crystallization transitions, and a higher glass transition temperature suggests superior thermal stability compared to compound **6**. Spirobifluorene core compounds **2** and **4** exhibit superior melting temperature in comparison with terthiophene-based compounds **6** and **7**. This can be ascribed to more flexible structure of terthiophene core, whereas spirobifluorene core restricts molecular motion due to its rigid and bulky configuration. In terms of glass transition temperatures, spirobifluorene core compound **2** showed highest value of 183 °C due to rigid and bulky configuration of spirobifluorene core and phenyldibenzofuran side unit. Overall, high glass transition temperatures of compounds **1-4**, **6**, **7** indicate enhanced film-forming characteristics, which are crucial for device layer fabrication

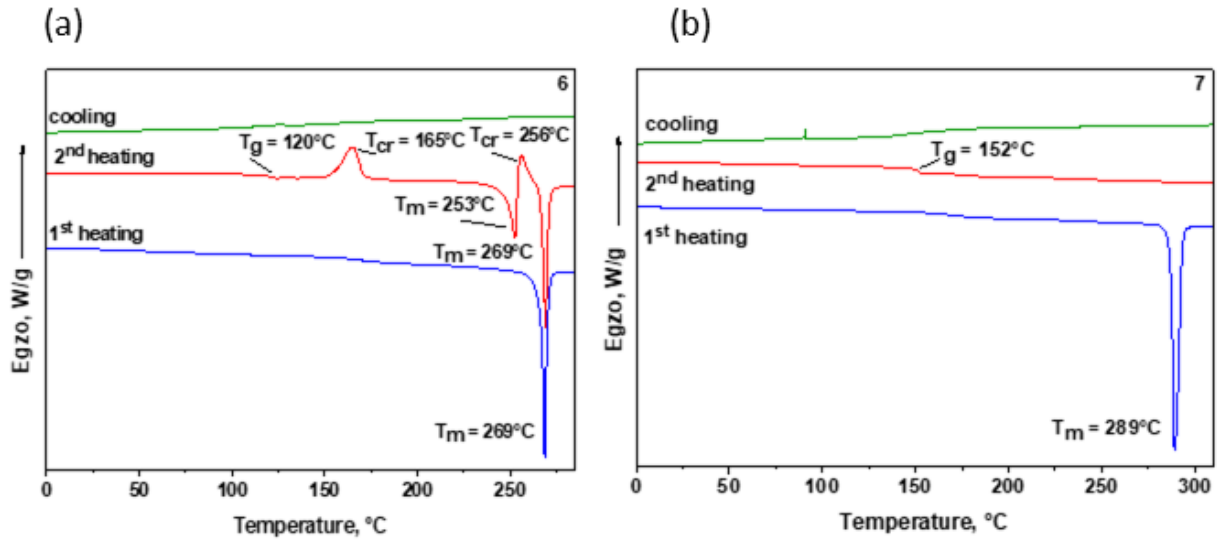

Fig. 20. DSC curves of compounds **6**(a), **7**(b).

2.2.2. Electrochemical Properties

Cyclic voltammetry (CV) was used to examine the electrochemical properties of the synthesized compounds **1-4**, **6, 7** (Figure 21). Reversible oxidation was observed within the 0 to +1.6V potential range for compounds **1-4**; similarly, compounds **6** and **7** showed reversible oxidations within the -1 to +1V potential range. No electrochemical degradation occurred that can be evidenced by new oxidation peaks on several scans for target compounds.

Phenylcarbazolyl disubstituted fluorenes **3** and **4** exhibit slightly lower ionization potentials compared to those of dibenzofuranyl disubstituted fluorenes **1** and **2** [59]. This characterization can be attributed to increased π-electron conjugation systems and stronger electron-donating properties of the fluorene derivatives.

Bis(carbazolyl)-substituted terthiophene (**6**) exhibits slightly lower ionization potential compared to carbazole-spirobifluorene derivative (**7**), owing to its more symmetric and highly conjugated structure, which promotes delocalization of π-electrons. The ionization potential (IP) values of compounds **1-4, 6, 7** established by CV were found to be in the short range of 5.38–6.27 eV.

Overall, dimethylfluorene and spirobifluorene core compounds exhibit higher IP values compared to terthiophene core compounds excluding compound **4**. This can be attributed to efficient π-conjugation and electron-rich terthiophene backbone, which promotes electron removal. Despite the small differences, overall, the determined IP values show that the compounds can be used in the active layers of OLEDs [60].

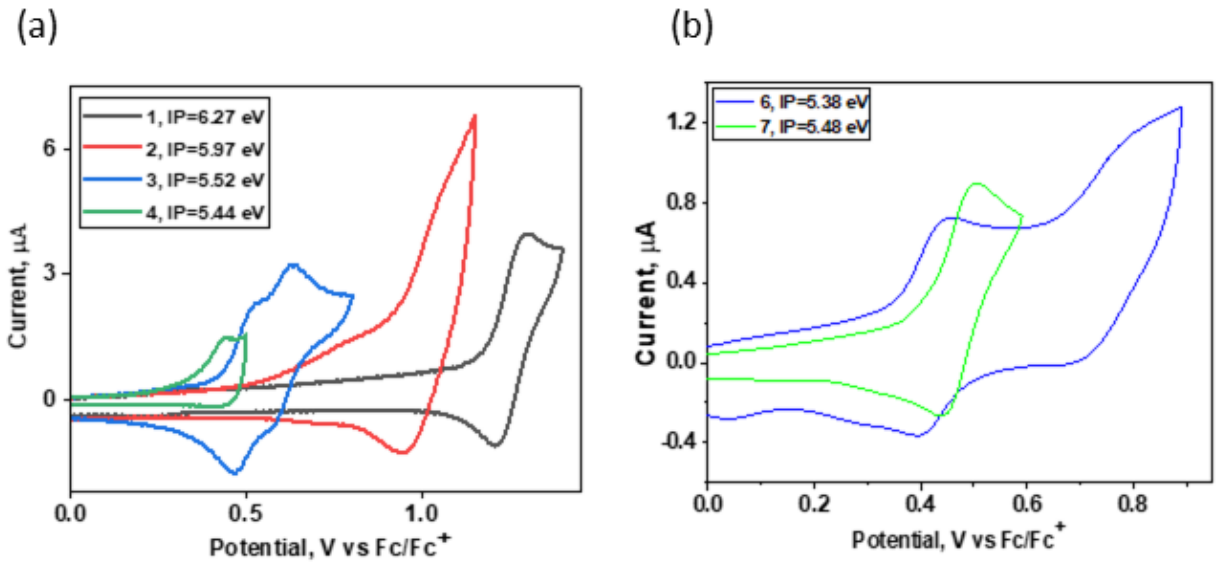

Fig. 21. Cyclic voltammograms of compounds **1-4**(a), **6-7**(b).

2.2.3. Photophysical Properties

The photophysical properties of compounds **1-4**, **6,** and **7** were established of toluene, THF, and thin films formed by solution process. As depicted in Figure 22a-b, normalized UV-Vis absorption spectra of the solutions of compounds **6** and **7** exhibit intense absorption bands in the near ultraviolet (UV) to blue-green visible region, while absorption of films of compounds **6** and **7** shifted toward longer wavelength. This bathochromic shift of films of compounds **6** and **7** can be ascribed to strong intermolecular interactions and π-π stacking of film samples. The PL spectra of toluene and THF solutions of compounds (Figure 24a-b) **6** and **7** indicate that emissions occur in the yellow region. Both compounds exhibit identical spectral shapes and the narrowest bandwidths, indicating that the emission originates from local (LE) singlet states and the effects of aggregation are not observed.

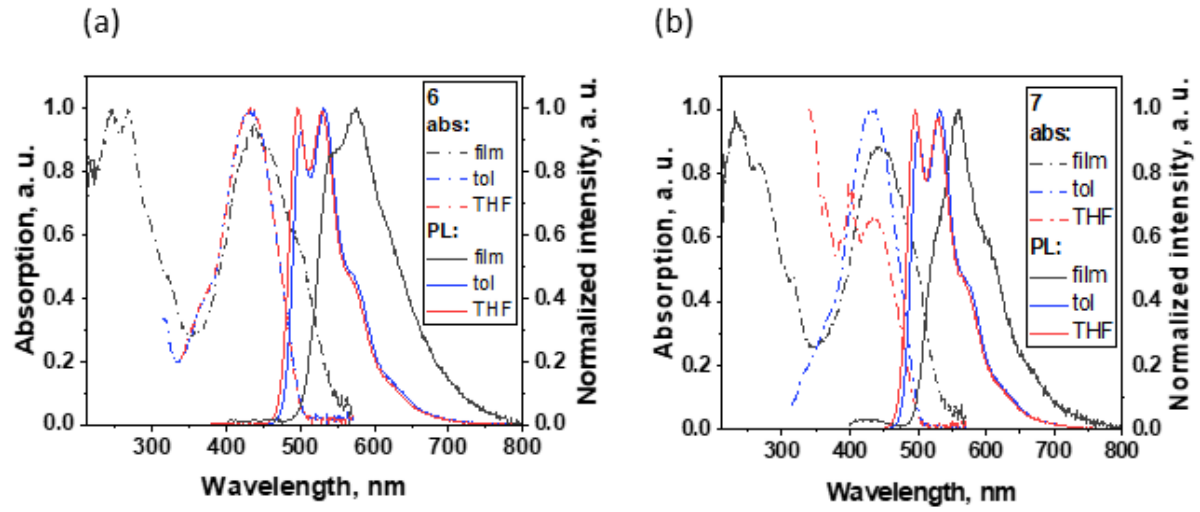

Fig. 22. UV-Vis absorption and PL spectra of films and solutions of compounds **6**(a) and **7**(b).

Time-resolved photoluminescence (TRPL, Figure 23) analysis of solutions of compounds **6** and **7** was conducted. It is evident that emission mainly arises from a emissive species in dilute solution, attributed to the mono-exponential fitting behavior of decay traces. The fluorescence lifetimes are in nanosecond range, which indicates a prompt fluorescence (LE) characteristic from organic luminophores. The PLQY (Table 2) values demonstrate that the emission efficiency of solutions of compounds **6** and **7** are significantly high, notably of THF. The polar solvent stabilizes the emissive excited state effectively and suppresses non-radiative relaxation pathways as evidenced by a significant enhancement in THF. PLQY value of film of compound **6** lower compared with that of compound **7**, confirming its molecular structure is more planar and highly conjugated, which enhanced π-conjugation enables effective π-electron delocalization.

Table 2. PLQY values of compounds **1-4**,**6**,**7**

PLQY values (%)				
Compound	**Thin film**	**Solution**		**mCP-tBu-doped (10 %) film**
		Toluene	**THF**	
1	46			
2	45			
3	25			
4	24			
6	8	30	78	25
7	12	49	90	46

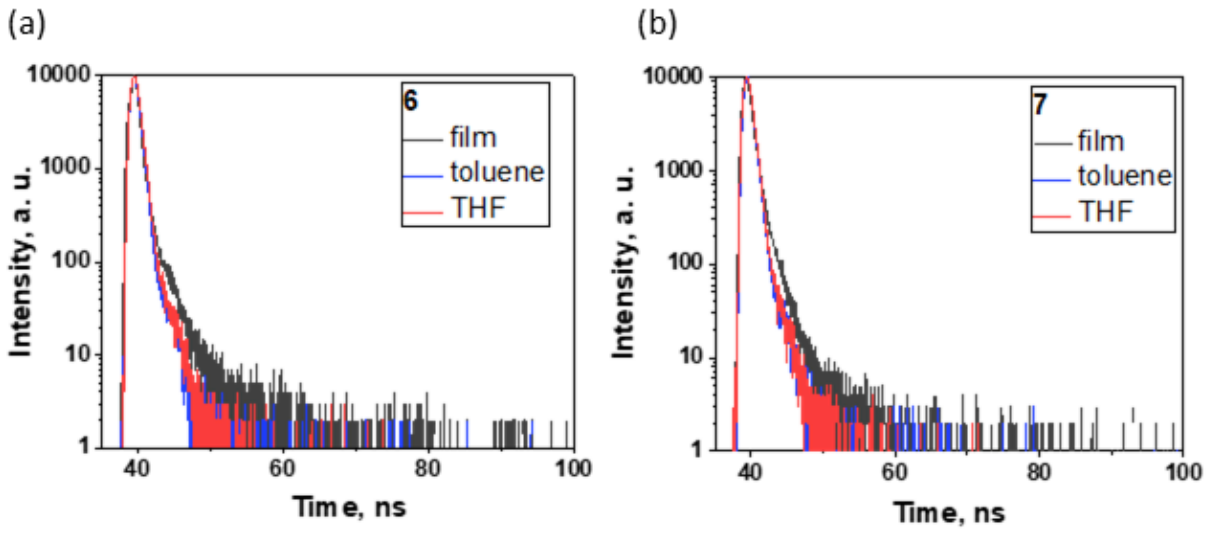

Fig. 23. TRPL decay curves of films and solution of compounds **6**(a) and **7**(b).

In comparison, thin films of the compounds **1-4 (**Figure 24) emit light in the blue region, indicated a shorter π-conjugation system of compounds **1** – **4** in comparison to that of compounds **6** and **7.**. This variation can be attributed to distinct structures of compounds **1-4**, **6**, **7**, where terthiophene core induced an efficient extended π-conjugation system that resulted in red-shifted emission for the thin films of compounds **6** and **7.**

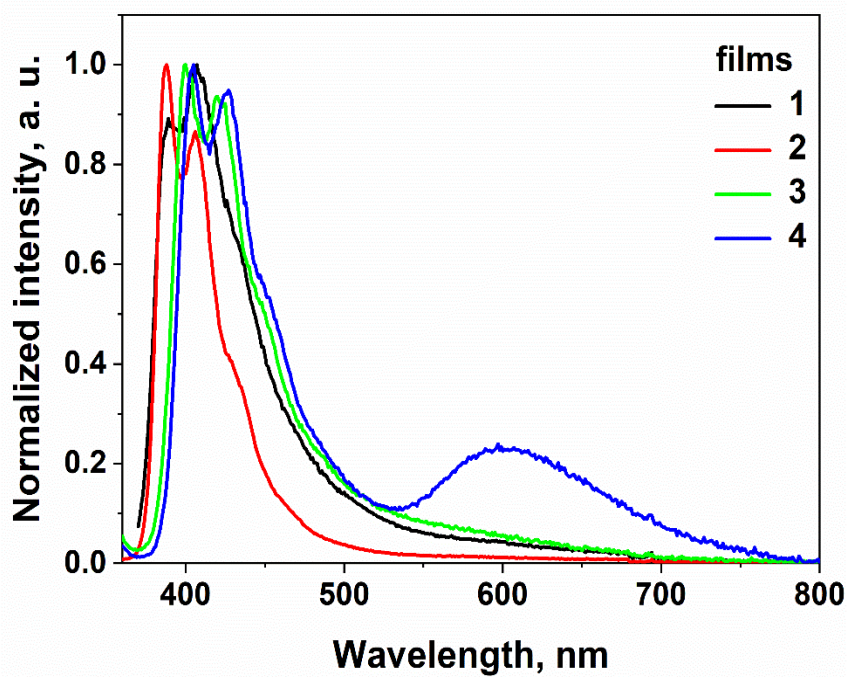

Fig. 24. PL spectra of films of compounds **1-4**.

TRPL analysis of thin films of compounds **1-4** (Figure 25), **6,** and **7** (Figure 23) was performed in order to determine the origin of the emission. Investigation of films of compounds **1-4** highlighted biexponential decay curves with fast components, in line with prompt fluorescence (LE) at 388-407 nm. The emission spectrum of the film of **4** exhibited the additional band peaking in the reddish-orange region of the spectrum at 605 nm [59], revealing triexponential decay includes a long-lived component, which may originate from the presence of aggregates due to π-π stacking, possibly indicating contribution of the intramolecular charge transfer (CT) interactions.

Compounds **1-4** are characterized as prospective materials for blue light-emitting devices. The PLQYs (Table 2) of thin films of compounds **1-4** are considerably higher compared to those of compounds **6** and **7**. Films of compounds **1** and **2** exhibit higher PLQYs compared to those of compounds **3** and **4**, which can be ascribed to efficient solid-state fluorescence and reduced aggregation-induced quenching.

The lower PLQYs of films of compounds **3** and **4** indicate more significant non-radiative deactivation. Conversely, compounds **6** and **7** have lower PLQYs of film despite their superior luminescence efficiencies of solutions. Significant variation can be assigned to high aggregation-induced quenching owing to stronger intermolecular π- π interactions [61].

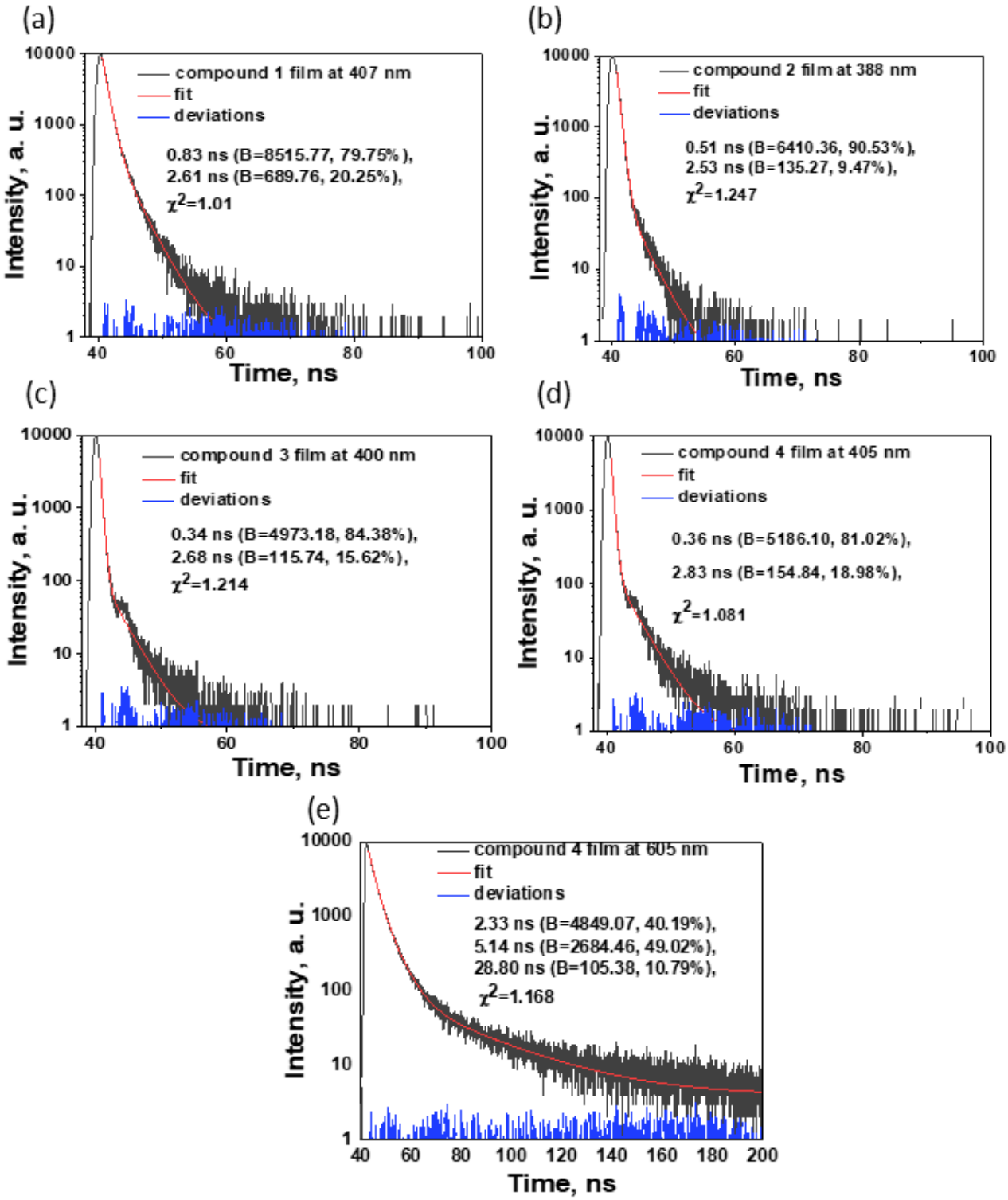

Fig. 25. TRPL decay curves of films of compounds **1-4**.

Additional investigation of mCP-tBu-doped films (Figure 26a) of compounds **6** and **7** indicates that film samples display luminescence in a broad green region. Both compounds exhibit nearly identical broad fluorescence spectra, which demonstrates comparable singlet excited states in the host matrix system. Time-resolved photoluminescence decay curves (Figure 26b,c) of both samples of compounds **6** and **7** are biexponential, as well as dominant prompt fluorescence components, suggesting excited-state relaxation pathways. By contrast, the sample of compound **7** shows an

enhanced PLQY (Table 2) value compared to that of compound **6** , which indicates more efficient fluorescence in the solid state. Under these conditions, compound **7** is a superior performing fluorescent emitter compared to compound **6**.

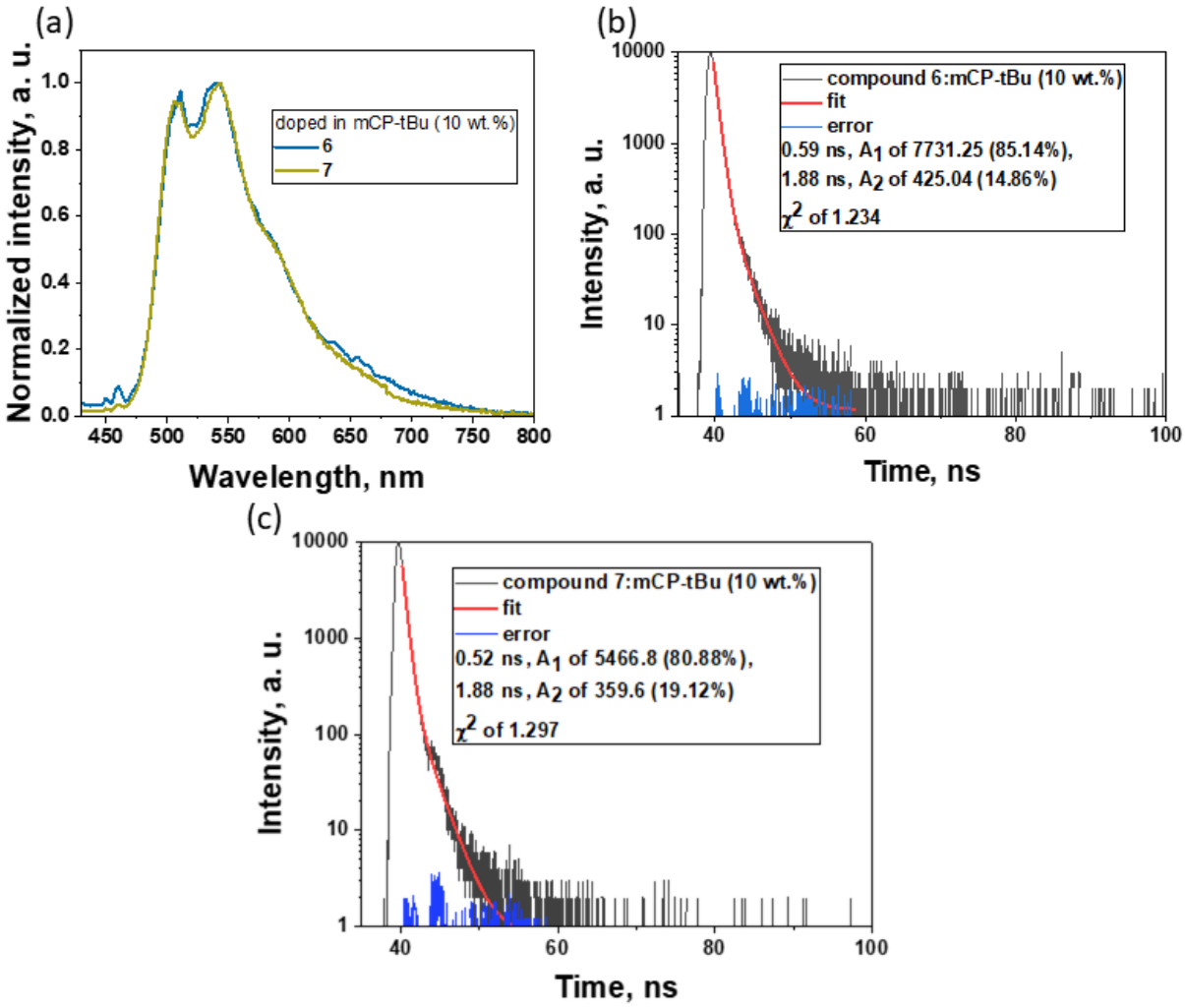

Fig. 26. PL spectra and TRPL decay curves of mCP-tBu-doped films of compounds **6** and **7**.

Overall phtophysical performance of both series of compounds is sufficient. The thin films of compounds **1-4** showed the best performance, with compounds **1** and **2** characterized by the highest PLQYs and thus have potential as blue fluorescent emitters.

2.3. Developments of OLEDs

2.3.1. Solution-processed OLEDs A and B

Emissive layer (EML) characteristics of spirobifluorene derivatives **2** and **4** were determined by fabricating solution-processed OLEDs A and B. The selection of spirobifluorene derivatives was based on various factors, including similarity of PLQY values of the films of compounds **1** and **2** (Table 2). Whereas, the PL spectrum of the film of compound **2** is significantly blue-shifted in comparison with the spectra of the films of compounds **1**, **3**, **4**. The OLED structures of devices A

and B are shown in Figure 27a. 1,4,5,8,9,11-Hexaazatriphenylenehexacarbonitrile (HAT-CN) was used for hole-injection layer (HIL) formation. 1,3,5-Tri(m-pyridin-3-ylphenyl)benzene (TmPyPb) was used for electron-transporting layer (ETL) formation. Compounds **2** and **4** was used for EML formation. Poly(9,9-dioctylfluorene-alt-N-(4-sec-butylphenyl)-diphenylamine) (TFB) was used for hole-transporting layer (HTL) formation.

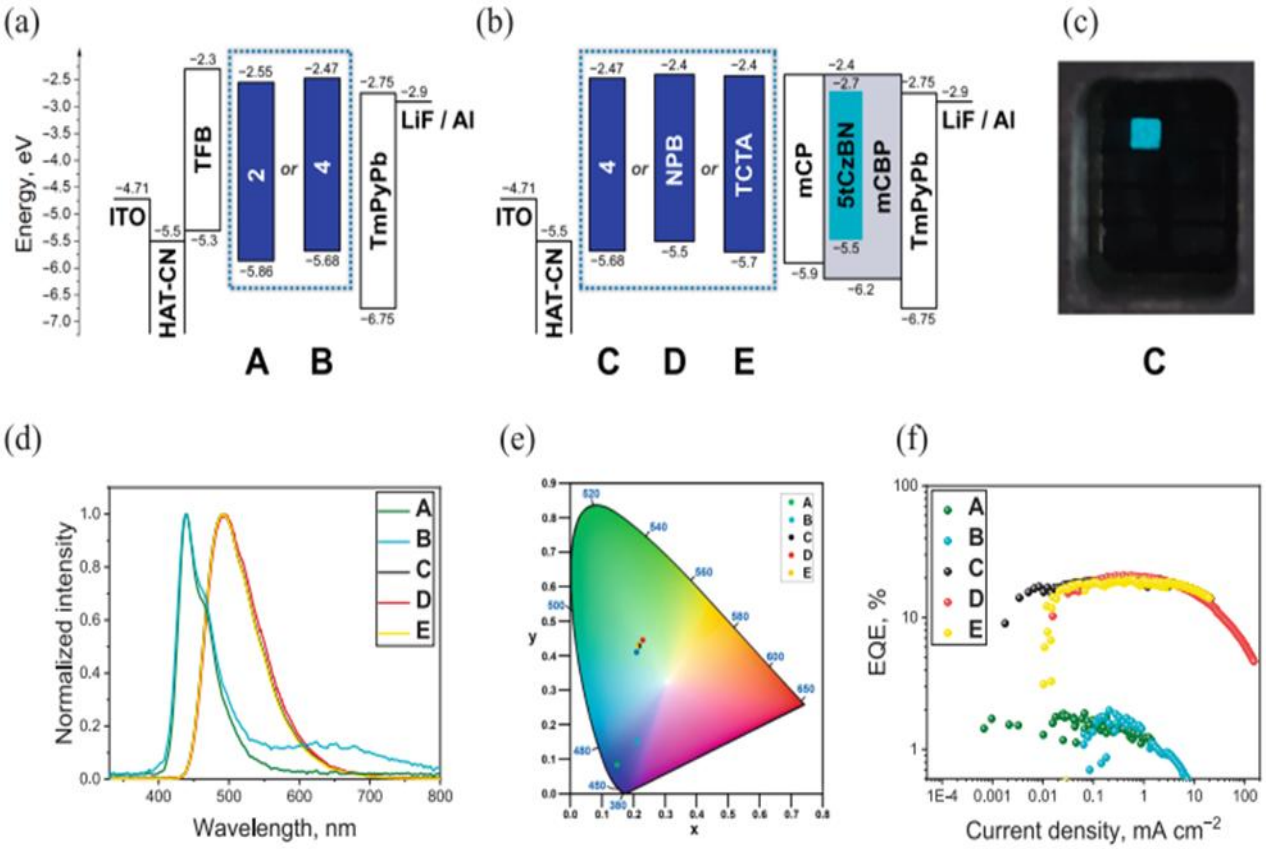

Fig. 27. Detailed structure and properties of A-E devices.

Device A exhibited the maximum EQE of 1.9% (Table 3, Figure 27f, Figure 28b). Device A demonstrated emission peak of the electroluminescence spectra at 439 nm wavelength (Figure 27d). The respective CIE color coordinates were 0.146 (x), 0.082 (y) (Figure 27e). The device B electroluminescence spectra displayed two peaks similar to the PL spectrum of compound **4**. A and B OLEDs exhibited bathochromically shifted emission peak positions in contrast to the PL bands of the compounds **2** and **4**.

The results obtained from these observations can be attributed to derivatives' dipole-dipole interactions with materials from OLEDs surrounding layers. The device B exhibited superior maximum EQE (Figure 28d) in comparison with device A, while the film of compound **4** demonstrated reduced PLQY as compared to the film of compound 2 (Table 3, Figure 27f, Figure 28).

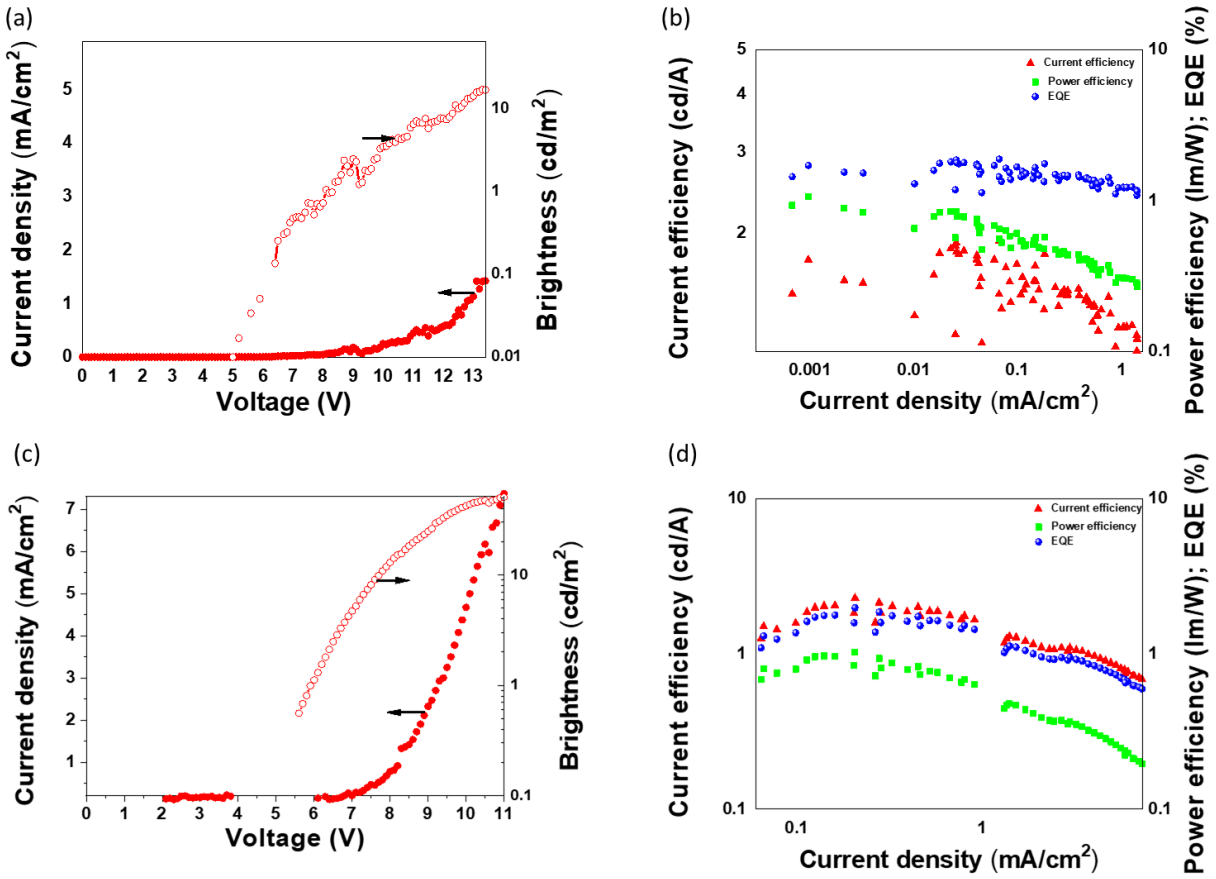

Fig. 28. Characteristic plots of device A(a,b), B(c,d),

In 2020, Feng et al [62], introduced four novel tetraphenylbenzosilole (TPBS) based emitters: TPBS-H, TPBS-F, TPBS-B, and TPBS-M (Figure 29, Table 3). Employing these compounds for emissive layer formation, nondoped OLEDs fabricated via a spin-coating technique with the configuration of poly(9,9-dioctylfluorene-co-N-(4-butylphenyl)-diphenylamine)(TFB) and 1,3,5-tri(m-pyrid-3-yl phenyl)benzene (TmPyPB) in which TFB and TmPyPB were used as hole-transporting and hole-blocking layers, respectively [62]. In comparison with the examined devices A and B (Figure 28a, c, Table 3), TPBS-based OLEDs exhibited low turn on voltages (2.8V) and superior current efficiencies ranging from 2.89 to 3.28 cd A^{-1} [62] (Table 3). Furthermore, TPBS-based devices characterized by higher power efficiencies with the values between 3.0 and 3.4 lm W^{-1} [62]. The EQE values of those materials, ranging between 3.1% and 3.6%, were higher than A and B devices [62]. TPBS-based devices exhibited stable deep-blue emission [62], whereas device B displayed shifted coordinates, suggesting less efficient stability of color.

Consequently, these results confirmed that devices A and B demonstrate lower overall performance with respect to TPBS-based OLEDs [62]. Despite the devices A and B serving as useful benchmarks, they still need further improvement to compete with the performance of reference OLEDs.

Table 3. OLEDs A-E performance results

OLED	HTL	EML	Turn-on voltage, V	Current efficiency, cd A^{-1}	Power efficiency, lm W^{-1}	EQE, %	CIEx,y	EL peak wavelength, nm
A	TFB	2	5.0	1.9/-/-	1.1/-/-	1.9/-/-	(0.14, 0.082)	439
B	TFB	4	5.6	2.3/-/-	1.0/-/-	2.0/-/-	(0.21, 0.156)	439, 623
C	4	5TCzBN: mCBP	2.9	52.3/50.4/41.8	43.3/18.2/9.6	19.7/19.1/ 15.8	(0.21, 0.430)	491
D	NPB	5TCzBN: mCBP	3.6	56.8/55.1/39.2	37.2/30.9/14.7	20.8/20.2/ 14.4	(0.22, 0.446)	493
E	TCTA	5TCzBN: mCBP	3.6	51.4/50.5/41.9	28.8/17.6/9.5	19.3/19.0/ 15.8	(0.21, 0.431)	491
[62]	TFB	TPBS-H	2.8	3.15	3.3	3.5	(0.15, 0.102)	438
[62]	TFB	TPBS-F	2.8	3.28	3.4	3.6	(0.15, 0.104)	438
[62]	TFB	TPBS-B	2.8	2.89	3.0	3.1	(0.15, 0.104)	438
[62]	TFB	TPBS-M	2.8	3.13	3.3	3.4	(0.15, 0.103)	438
[64]	TATT	5TCzBN: mCBP	2.79	45.5	34.1	17.4	-	490
[64]	4DBTHPB	5TCzBN: mCBP	2.76	44.3	33.8	17.0	-	490
[64]	4DBFHPB	5TCzBN: mCBP	2.74	45.2	36.1	17.3	-	490

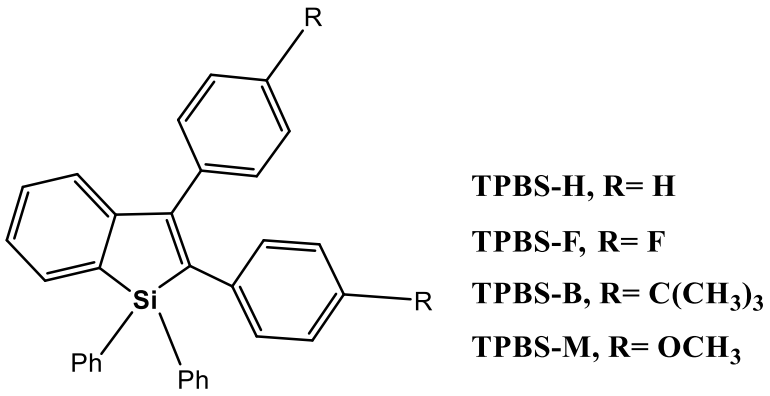

Fig. 29. Structure of TPBS-based compounds [62],

2.3.2. OLEDs C-E with 5tCzBN fabricated by thermal vacuum evaporation

Compound **4** was examined fabricating additional OLED series, which were constructed by the thermal vacuum evaporation method (Figure 27b-e, Figure 32). Compound **4** used as hole transporter in device C, N,N′-di(1-naphthyl)-N,N′-diphenyl-(1,1′-biphenyl)-4,4′-diamine (NPB) in device D, and tris(4-carbazoyl-9-ylphenyl)amine (TCTA) in device E (Table 3, Figure 27b). 1,3-Bis(N-carbazolyl)benzene (mCP) was used for electron-blocking layer (EBL) formation. High-performance sky-blue TADF light emitting material 2,3,4,5,6-pentakis(3,6-di-tert-butyl-9H-carbazol-9-yl)benzonitrile (5tCzBN) was used to be doped in 3,3′-di(9H-carbazol-9-yl)-1,1′-biphenyl (mCBP),

which is commonly employed host material for TADF and Phos OLEDs [63]. The low turn-on voltages, in combination with the consistency detected between the C-E devices' electroluminescence spectra and the 5TCzBN [63] PL spectrum, suggest that the device architecture was appropriately designed and the charge balance on the recombination sites was efficient (Table 3, Figure 27b-e).

In 2020, Kamata et al [64], reported three hexaphenylbenzene (HPB) based HTLs, namely **TATT**, **4DBTHPB**, and **4DBFHPB** (Figure 30).

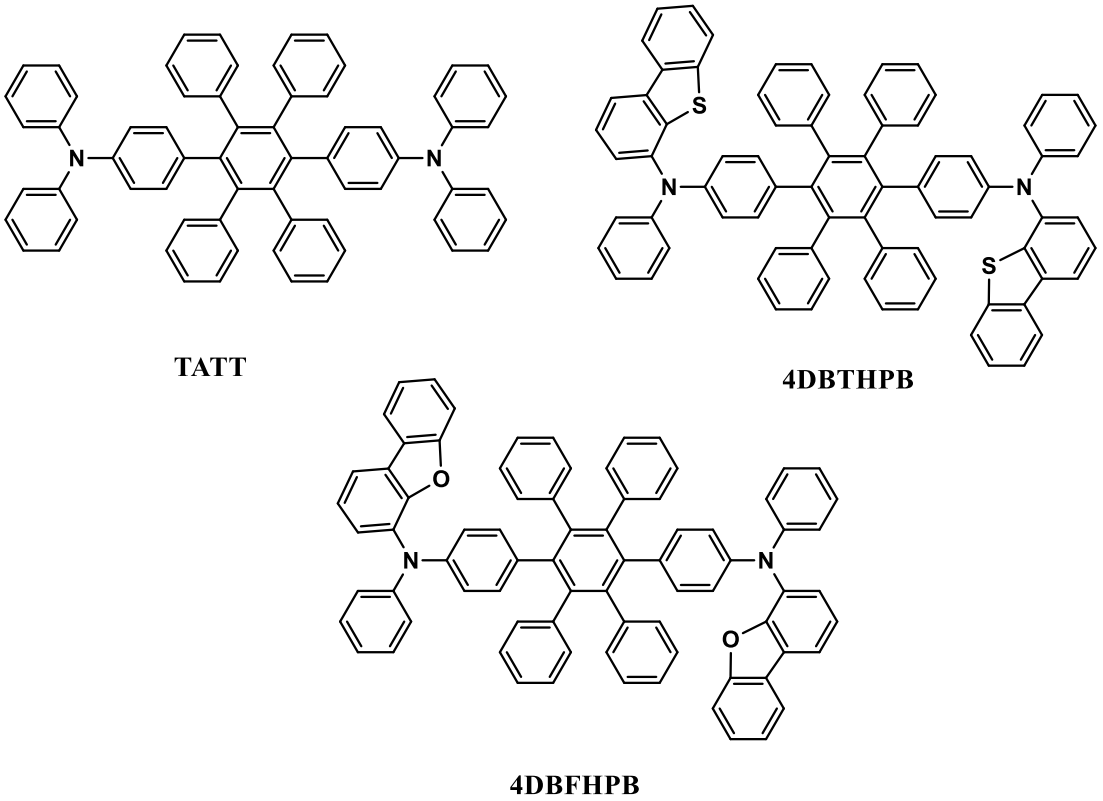

Fig. 30. Structure of **TATT**, **4DBTHPB**, and **4DBFHPB** compounds [64].

A series of OLEDs was fabricated using the thermal vacuum evaporation technique (Figure 31, Table 3), in which TATT, 4DBTHPB, and 4DBFHPB were used as HTL [64]. In comparison with device C, 5TCzBN-based sky-blue TADF OLEDs exhibited similar turn on voltages ranging from 2.8 to 2.9 V [64]. The current efficiency of device C, 52.3 cd A^{-1} exceeded the values obtained for 5TCzBN-based TADF OLEDs (44.3–45.5 cd A^{-1}) [64]. Furthermore, device C exhibited superior power efficiency with the value of 43.3 lm W-1, enhanced performance compared to 5TCzBN-based devices [64].

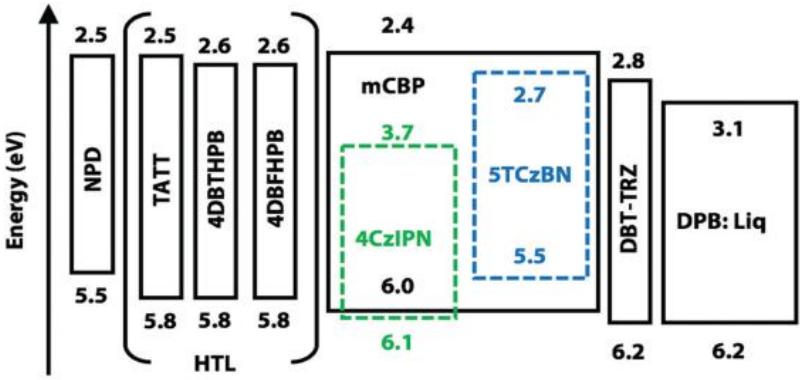

Fig. 31. Structure of **TATT**, **4DBTHPB**, and **4DBFHPB** based OLEDs [62].

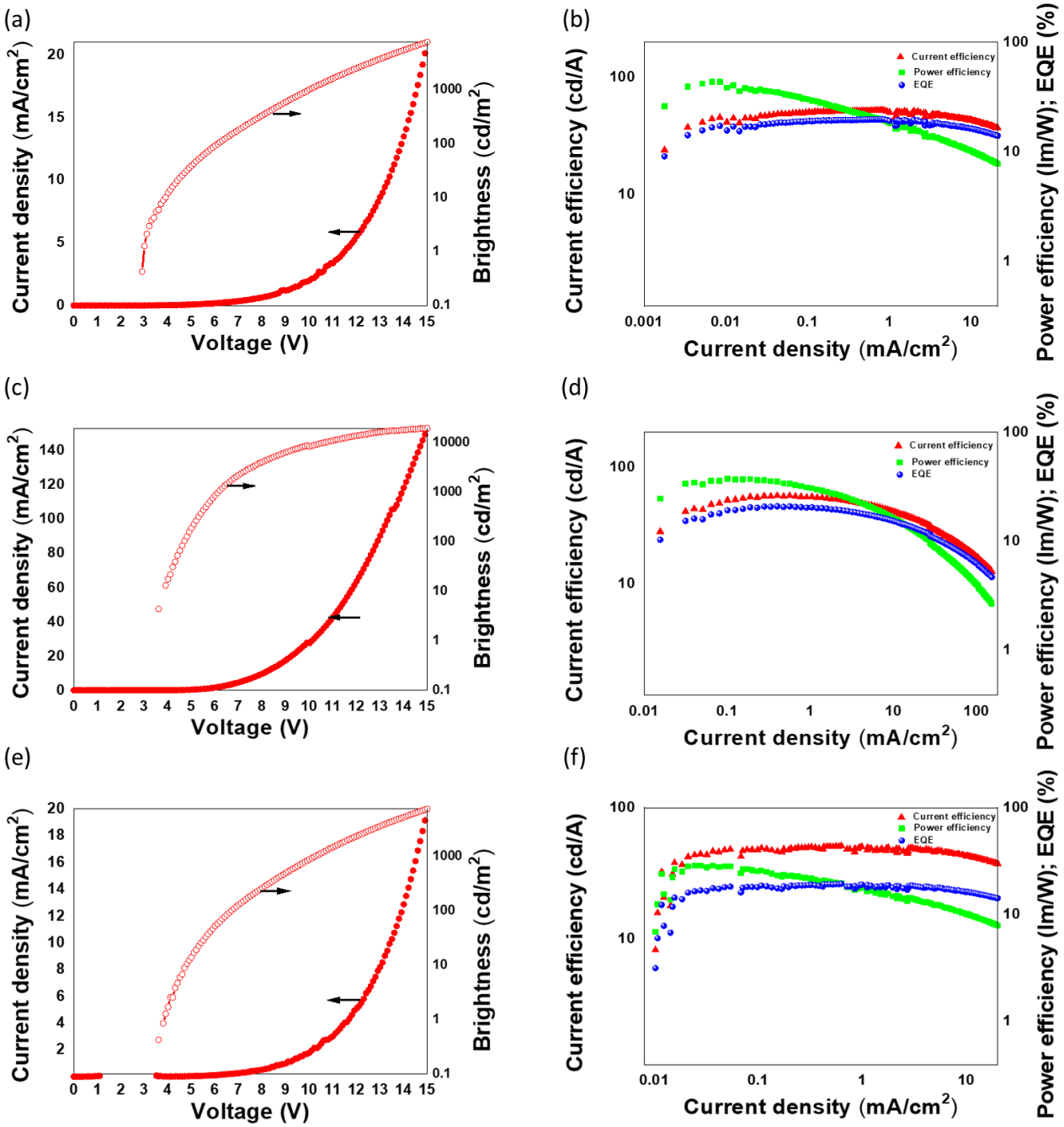

Fig. 32. Characteristic plots of device C (a,b), D (c,d), E (e,f)

The C device with a EQE value of 19.7%, demonstrated higher value than those of 5TCzBN-based counterparts [64]. C and 5TCzBN-based devices characterized by identical emission peaks at 490 nm and 491 nm, respectively, confirming sky-blue emission from the 5TCzBN:mCBP emitting layer [64]. Overall, the obtained results indicate that device C was characterized by enhanced performance compared to 5TCzBN-based TADF OLEDs [64].

Overall, the observations indicate that the compound spirobifluorene-based compound **4** can efficiently be utilized in the active layers of OLEDs.

2.4. Summary of Properties

As confirmed by the observed properties, both the attached peripheral donor units carbazole, dibenzofuran, and central moieties dimethylfluorene, spirobifluorene, and terthiophene influence the main thermal, photophysical, and electrochemical properties of the synthesized compounds. The compound containing the spirobifluorene donor unit attached to the terthiophene-core demonstrated superior thermal stability with the 5% weight loss temperature of 483 °C. The fluorene-core compounds exhibited blue emission, while the terthiophene-core compounds displayed emission in the yellow color region. These findings are consistent with the main characteristics of fluorene and terthiophene compounds. Furthermore, compounds containing phenylcarbazole exhibited more redshifted emission than those of the compounds attached to phenyldibenzofuran peripheral unit. The compound containing dimethlyfluorene central unit and phenyldibenzofuran donor exhibited the highest PLQY value, which may originate from the rigid planar biphenyl configuration of fluorene and localized flexibility of phenyldibenzofuran unit. The OLED based on spirobifluorene core and phenylcarbazole donor compound showed the highest EQE than others due to enhanced π-electron conjugation system and better aligment of IP value between adjacent layers, which promote hole injection and transport, reducing energy barriers and enhancing device performance.

Overall, further modifications of these compounds can be performed to improve characteristics of compounds. For instance, spirobifluorene may be employed as donor fragment for enhancing thermal stability, while phenyldibenzofuran or terthiophene can be used as central moieties to improve flexibility, and expantion of π-conjugation system, thus preserve suitable properties for OLED devices.

3. Engineering part

3.1. Recommendations

The technological scheme for the production of 50 kg per batch of the dimethylfluorene-based compound **1** is illustrated below (Scheme 3).

The manufacturing process of target compound **1** consists of three primary steps. The first section involves the reaction of reactants under an inert atmosphere in a batch reactor and liquid-liquid extraction using DCM and distilled water, followed by solvent evaporation. The second section covers purification by column chromatography, followed by purified final product isolation through final solvent evaporation. The final section comprises obtaining the product as a solid through crystallization and drying of the purified target compound. In the first main stage of the production process, 32.42 kg 2,7-dibromo-9,9-dimethyl-9H-fluorene (**a)** and 59.7 kg (6-phenyldibenzo[b,d]furan-4-yl)boronic acid (**b)** were introduced to the 3 m^3 glass batch reactor **R,** which is equipped with a heating jacket and agitator driven by electric motor **M,** followed by the addition of 1.95 m^3 DMF solvent to dissolve the raw materials, which was controlled through manual globe valves. The hot water was used as a heating medium for the jacket. Thereafter, the mixture was stirred under vacuum for 20 minutes using a dry screw vacuum pump, and subsequently was purged with inert argon gas from a stream of gas cylinder **A** to create an inert atmosphere for the prevention of catalyst deactivation. Bis(triphenylphosphine) palladium(II) dichloride (1.3 kg) was added to the reaction vessel from stream **c,** and then the mixture was stirred for 15 minutes. Potassium carbonate solution (0.33 m^3) from stream **d** was introduced to the reactor. The reaction mixture was stirred at 80 °C for 24 hours. After the reaction was completed, the reactor was cooled to ambient temperature. The obtained product solution was transferred to the extraction column **E** by an air-operated double diaphragm pump, with a capacity of 223 l/min. The extraction column was supplied with DCM and distilled water to establish a distinct two-phase liquid separation. The solution was collected from the extraction column **E** and transferred to the wiped film evaporator **WF1**, while the aqueous phase was directed to the water recovery unit. The purified water was reused in the extraction column **E**. The solution was concentrated in the evaporator **WF1,** while the released DCM vapors throughout the process were directed to the condenser **N** to be used back in the extractor **E**. The compound was adsorbed onto the silica surface inside the evaporator **WF1** after adding silica gel and then fully evaporated to form a dry powder for further processing. Afterward, a dry powder was collected in storage **S1** and manually transferred to the fixed-bed column **C**.

In the second main stage of the production process, removal of leftover impurities in the target compound was conducted in a fixed bed column **C** using a THF/hexane (1:2, w/w) as an eluent. The absorption bed of the column is made of silica gel. Subsequently, the purified target compound fraction was forwarded to the wiped film evaporator **WF2** using a UV detector from fixed bed column **C**, while the released vapors of the eluent were redirected to the eluent regeneration process unit. The regenerated eluent was then supplied to column **C**.

The final step of the production process was crystallization of the target compound in the crystallizer unit **CR**. The residual solvent and moisture were removed from the resulting final product in dryer **D**. The final dry solid material, 50 kg per batch, from vacuum dryer **D** was collected in storage vessel **S2**.

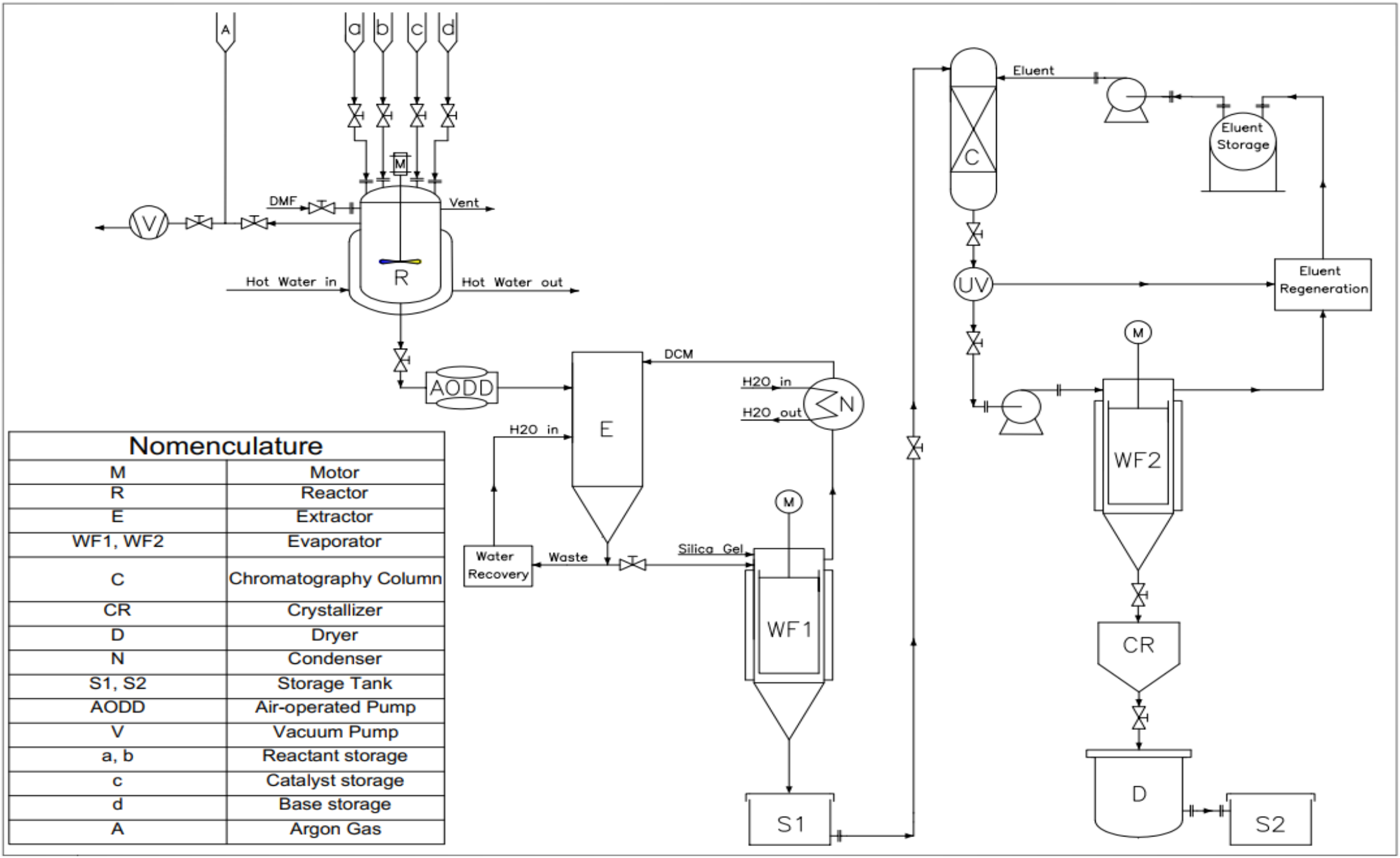

Nomenculature	
M	Motor
R	Reactor
E	Extractor
WF1, WF2	Evaporator
C	Chromatography Column
CR	Crystallizer
D	Dryer
N	Condenser
S1, S2	Storage Tank
AODD	Air-operated Pump
V	Vacuum Pump
a, b	Reactant storage
c	Catalyst storage
d	Base storage
A	Argon Gas

Scheme 3. Technological scheme of target compound **1**

4. Safety and health of employees

4.1. Occupational Safety and Health

4.1.1. Occupational risk factors

The chemical industry is exposed to harmful and dangerous risk factors that can affect the employee‘s life, can cause danger to their body, or result in occupational disease. 6 main groups of risk factors regarding the safety and health of employees can be characterized:

1) Physical risks: noise, vibration, temperature changes
2) Mechanical risks: a factor regarding a danger due to improper installation of the workplace, work equipment, and their moving parts, additionally, due to possible explosion, fire or failure to ensure the stability and strength of structures
3) Chemical risks: a chemical element or compound that poses a risk to human health or life, such as toxic, corrosive or flammable substances
4) Biological risks: microorganisms, including genetically modified ones, cell cultures, human endoparasites, which may lead to infection, allergy, poisoning to the employee
5) Psychosocial risks: factors such as working conditions, requirements, organization, and employee relationships that lead to mental stress to the employee
6) Ergonomic risks: factors such as workload, stress, and adapting the workplace to the capabilities of the employee [65]

4.1.2. Personal protective equipment

Personal Protective Equipment is a device intended for a worker to wear or have in order to protect himself/herself from risk factors that may pose a threat to the safety and health of the worker. Personal protective equipment must be used when the risk cannot be avoided or sufficiently reduced by collective protective measures, work organization measures, methods, or procedures [66]. Personal protective equipment can be characterized into groups:

- Eye and/or face protection: This group includes safety glasses and googles with side shields. Eye and face protection must be worn according to tested and approved strandards such as NIOS (USA) and EN 166 (EU)
- Skin protection: This group includes gloves. Gloves must be inspected before use to check whether the gloves are not torn and are suitable for use. To avoid skin contact with chemicals, the glove removal method must be followed without touching the outer surface of the gloves. In accordance with the applicable legislation and proper laboratory practice, the used gloves must be disposed. Hands must be washed and dried. Protective gloves must be in accordance with the requirements of Regulation (EU) 2016/425 and standard EN374.
- Body protection: Protection against chemicals by use of complete set of protective chemical and flame-resistant antistatic clothing. Protective equipment type must be selected taking into account the quantities and concentrations of hazardous substances in the workplace.

- Respiratory protection: This group includes respirators. The full-face respirator with multipurpose cartridges must be used when a risk assessment implies that the air purifying respirators are appropriate. The full-face respirator must be used when the respirator is the only protection measure. The respirators must be used that have been tested and approved in accordance with NIOSH (US) or CEN(EU)

- Environmental protection: if it is safe to do so, all possible measures must be taken to prevent chemical leaks and spills, and chemicals must be prevented to enter the drain[65].

4.1.3. Fire prevention measures

Appropriate extinguishing media must be selected throughout the event of fire. If necessary, a self-contained breathing apparatus must be used. The extinguishing agents which are given below may be used for firefighting[66]:

- water spray;
- alcohol-resistant foam;
- dry chemical powder;
- carbon dioxide.

The laboratory space should be properly ventilated before and after completing work [66]. In case of fire, the fire prevention service must be immediately informed by the student by calling the emergency number „112“, and the laboratory work supervisor must be informed. Carbon dioxide extinguishers are used for all operating electrical equipment [66].

4.1.4. First aid measures

- In case of inhalation of a chemical or its vapors, if the affected person is breathing, move him/her to fresh air. If the affected person is not breathing, apply artificial respiration. Seek medical attention.
- In case of skin contact with a chemical, wash the skin with soap and plenty of water. Seek medical attention
- If a chemical gets into the eyes, rinse them thoroughly with plenty of water for at least 15 minutes. Seek medical attention
- In case of swallowing a chemical, do not induce vomiting and avoid giving anything to an unconscious person. Rinse mouth with plenty of water. Seek medical attention

4.1.5. Characteristic of designed materials

a) Company location: research laboratory concerning the development of semiconductors , Department of Polymer Chemistry and Technology, KTU Santaka Valley, Kaunas.

b) Corporate objective: Providing educational and related services to develop individuals with globally competitive research abilities as well as delivering support to the international community through innovations that improve life quality

c) Materials used: 2,7-dibromo-9,9-dimethyl-9H-fluorene, 2,7-dibromo-9,9’-spirobifluorene, (9-phenyl-9H-carbazol-3-yl)-boronic acid, (6-phenyldibenzo[b,d]furan-4-yl)boronic acid, 5,5"-dibromo-2,2':5',2"-terthiophene, (9-phenyl-9H-carbazol-2-yl)boronic acid, (9,9'-spirobi[fluoren]-2-yl)boronic acid, bis(triphenylphosphine) palladium(II) dichloride, dimethyl sulfoxide, dichloromethane, ethyl acetate, nefras 80/120, toluene, dimethylformamide, hexane, acetone, tetrahydrofuran, sodium sulfate, potassium carbonate, argon.

d) Synthesized materials:

- Compound **1**: 6,6'-(9,9-Dimethyl-9H-fluorene-2,7-diyl)bis(4-phenyldibenzo[b,d]furan)
- Compound **2**: 2,7-Bis(6-phenyldibenzo[b,d]furan-4-yl)-9,9'-spirobi[fluorene]
- Compound **3**: 3,3'-(9,9-Dimethyl-9H-fluorene-2,7-diyl)-bis(9-phenyl-9H-carbazole)
- Compound **4**: 2,7-Bis(9-phenyl-9H-carbazol-3-yl)-9,9'-spirobi[fluorene]
- Compound **5**: 2-(5"-Bromo-[2,2':5',2"-terthiophen]-5-yl)-9-phenyl-9H-carbazole
- Compound **6**: 5,5"-Bis(9-phenyl-9H-carbazol-2-yl)-2,2':5',2"-terthiophene
- Compound **7**: 2-(5"-(9,9'-Spirobi[fluoren]-2-yl)-[2,2':5',2"-terthiophen]-5-yl)-9-phenyl-9H-carbazole

4.1.6. Occupational risk assessment

a) Chemical agents

Table 4. Hazardous properties of materials

Compound	Hazard symbol	Classification of the substance or mixture
2,7-Dibromo-9,9-dimethyl-9H-fluorene		Skin Corrosion/Irritation (Category 2 (H315)), Serious Eye Damage/Eye Irriration (Category 2 (H319)), Specific target organ toxicity-(single exposure) (Category 3 (H335))
2,7-Dibromo-9,9’-spirobifluorene		May cause an allergic skin reaction (H317), Causes serious eye irritation (H319)
(9-Phenyl-9H-carbazol-3-yl)-boronic acid		Skin Corrosion/Irritation (Category 2 (H315)), Serious Eye Damage/Eye Irriration (Category 2 (H319)), Specific target organ toxicity-(single exposure) (Category 3 (H335))
(6-Phenyldibenzo[b,d]furan-4-yl)boronic acid		Harmful if swallowed (H302) Skin Corrosion/Irritation (Category 2 (H315)), Serious Eye Damage/Eye Irriration (Category 2 (H319)), May cause respiratory irritation (H335)
5,5"-Dibromo-2,2':5',2"-terthiophene		Toxic if swallowed (H301), Skin Corrosion/Irritation (Category 2 (H315)), Causes serious eye damage (H318), May cause respiratory irritation (H335)

Compound	Hazard symbol	Classification of the substance or mixture
(9-Phenyl-9H-carbazol-2-yl)boronic acid		Acute toxicity, oral (Category 4 (H302)), Skin Corrosion/Irritation (Category 2 (H315)), Serious Eye Damage/Eye Irriration (Category 2A (H319)), Acute toxicity, inhalation (Category 4), Specific target organ toxicity-(single exposure) (Category 3 (H335))
Bis(triphenylphosphine) palladium(II) dichloride		Harmful if swallowed (H302), Harmful in contact with skin (H312), Skin Corrosion/Irritation (H315), Eye Damage/Eye Irriration (H319), Harmful if inaled (H332), May cause respiratory irritation (H335), May cause long-lasting harmful effects to aquatic life (H413)
(9,9'-Spirobi[fluoren]-2-yl)boronic acid		Skin corrosion/irritation (Category 2), Serious eye damage/eye irritation (Category 2A)
Dimethylsulfoxide		Combustible liquid (H227), Acute toxicity, skin corrocion/irritation, serious eye damage/eye irritation, respiratory or skin sensitization
Dichloromethane,		Skin Corrosion/Irritation (Category 2 (H315)), Serious Eye Damage/Eye Irriration (Category 2 (H319)), Carcioneginicity (Category 2 (H351)), Specific target organ toxicity (H336)
Ethyl acetate		Highly flammable liquid and wapor (H225), Eye Damage/Eye Irriration (H319), May cause drowsiness or dizziness (H336)
Nefras 80/120		Highly flammable liquid and vapor (H225), May be fatal if swallowed and enters airways (H304), May cause drowsiness or dizziness (H336), May cause long-lasting harmful effects to aquatic life (H411)
Toluene		Highly flammable liquid and vapor (H225), May be fatal if swallowed and enters airways (H304), Skin Corrosion/Irritation (H315), May cause drowsiness or dizziness (H336), Suspected of damaging the unborn child (H361d), May cause damage to organs through prolonged or repeated exposure (H373)

Compound	Hazard symbol	Classification of the substance or mixture
N-N-Dimethylformamide		Flammable liquid and vapor (H226), Harmful in contact with skin or if inhaled (H312+H332), Eye Damage/Eye Irriration (H319), May damage the unborn child (H360D)
Hexane,acetone		Highly flammable liquid (H225), Aspiration hazard (Category 1 (H304)), Specific target organ toxicity, central nervous system, single and repeated exposures (H336+ H373), Long-term chronic aquatic hazard (H412)
Tetrahydrofuran		Highly flammable liquid (Category 2 (H225)), Acute toxicity, oral (Category 4 (H302)), Eye Damage/Eye Irriration (Category 2 (H319))
Sodium sulfate		Acute toxicity, Eye Irriration
Potassium carbonate		Skin Corrosion/Irritation (Category 2 (H315)), Serious Eye Damage/Eye Irriration (Category 2 (H319)), Specific target organ toxicity (H335)
Argon		Gases under pressure (compressed gas (H280))

b) Physical factors

Table 5. Standard and lab reading values regarding physical factors

Factors	Values standards	Lithuania standards
Thermal environment	Warm period: 22.8 ℃ to 26.1℃ Cold period: 20℃ to 23.9℃ [67]	HN 69:2003
Noise	L_{ex}, 8h = 85 dBA, L_{cpeak} =137dbc [68]	HN 33:2011
Air pollution	(8 OU_E/m^3) [69]	HN 23:2011
Illumination	1000 lumens/m^2 [70]	HN 98:2014
Equipment grounding	TT-system TN-system IT system	(Elektros įrenginių įrengimo taisyklės. Vilnius, 2000. 487 p [71,72] Saugos taisyklės eksploatojant elektros įrenginius, Valstybės žinios, 2001, nr. 110-4008) [72]

4.1.7. Hygiene standards

Table 6. Working hygiene standards

Factors	Analyzed working standard	Lithuanian Standard
Thermal environment	Warm period: 22 ℃ to 24 ℃ Cold period: 21 ℃ to 23 ℃	HN 69:2003
Noise	L_{EX},8h = 95 dBA Lcpeak = 130 Dbc	HN 33:2011
Illumination	150-205 lumens/m^2	HN 98:2014
Equipment grounding	TT-system	[71, 73]

Lithuanian hygiene standards regarding the limit values of occupational exposure to chemicals are determined by long-term exposure limit (LPRD) or reference period of 8 hours and short-term exposure limit (TPRD) or reference period of 15 minutes. Data regarding to exposure limits of certain chemicals are given in Table 6.

Table 7. Occupational exposure limits for chemicals [69]

Chemical substance	Threshold size						Indications of health effects
	LPRD		TPRD		Limit value not to be exceeded		
	mg/m^3	ppm	mg/m^3	ppm	mg/m^3	ppm	
Tetrahydrofuran	150	50	300	100	-	-	O
Dimethylsulfoxide	150	50	500	150	-	-	O
N,N-dimethylformamide	15	5	30	10	-	-	RO
Ethyl acetate	500	150	-	-	1100	300	-
Acetone	1210	500	2420	1000	-	-	O
Toluene	192	50	384	100	-	-	RO
n-Hexane	72	20	-	-	-	-	R

R= toxic for reproduction, O = the substance can penetrate through the body

Conclusions

1. New derivatives of 2,7-dibromo-9,9-dimethyl-9H-fluorene, 2,7-dibromo-9,9’ spirobifluorene and derivatives of 5,5''-dibromo-2,2':5',2''-terthiophene have been successfully synthesized. The structures of synthesized compounds were confirmed by ^{1}H NMR spectroscopy and MS spectrometry.
2. Thermal, photophysical, and electrochemical properties were investigated:
   2.1. All synthesized compounds were determined to be thermally and morphologically stable. Their 5% weight-loss temperatures range from 430 °C to 483 °C, and glass transition temperatures were recorded in the range of 120-183 °C. The larger destruction and glass transition temperatures are characterized by the compound containing a spirobifluorene functional group due to its higher molecular mass.
   2.2. It was evaluated that synthesized terthiophene-based compounds absorb UV light within the range of up to 445 nm. The synthesized compounds with spirobifluorene and dimethylfluorene core emit light in the blue region, meanwhile, terthiophene core compounds exhibit emission in the yellow region due to strong intermolecular interactions and π-π stacking. The quantum yield of film of compound with dimethylfluorene core and phenyldibenzofuran functional unit was higher than those of other compounds, with the value of 46%
   2.3.The electrochemical properties determined from cyclic voltammetry demonstrate that all compounds are electrochemically stable. The ionization potentials were found to be broadly similar, ranging from 5.38 to 6.27 eV. The obtained electrochemical behaviour demonstrate that the compounds can be used in the active layers of OLEDs.
3. The technological scheme of production of 6,6'-(9,9-dimethyl-9H-fluorene-2,7-diyl)bis(4-phenyldibenzo[b,d]furan is proposed.

List of publications

1. KALATOZISHVILI, Akaki; KERUCKIENE, Rasa; NAGHIZADE, Rashad; BEZVIKONNYI, Oleksandr; VOLYNIUK, Dmytro, et al. Hole-Transporting Deep Blue Emissive Derivatives of Fluorene and Dibenzofuran Or Carbazole for Organic Light Emitting Diodes. Elsevier BV, -03-04, 2026.
2. Rashad Naghizade, A. Kalatozishvili, R. Keruckiene, J. V. Grazulevicius, Derivatives of 2,7-Dibromo-9,9-Dimethyl-9H-Fluorene and 2,7-Dibromo-9,9 Spirobifluorene as Electroactive Materials // Chemistry and Chemical Technology 2025. Student Scientific Conference, Lithuania. Vilnius: Vilnius University Press. 2025.

List of references

1. C., Amruth; PAHLEVANI, Majid and WELCH, Gregory C. *Organic Light Emitting Diodes (OLEDs) with Slot-Die Coated Functional Layers.* Royal Society of Chemistry (RSC), -12-16, 2020.
2. NAYAK, Debashish and CHOUDHARY, Ram B. *A Survey of the Structure, Fabrication, and Characterization of Advanced Organic Light Emitting Diodes.* Elsevier BV, -04-01, 2023.
3. NHARI, Laila M.; EL-SHISHTAWY, Reda M.; LU, Qiuchen; LI, Yuanzuo and ASIRI, Abdullah M. *Novel Triarylamine-Based Hole Transport Materials: Synthesis, Characterization and Computational Investigation.* MDPI AG, -06-07, 2021.
4. MEER, Bushra B.; SHARMA, Dhruv; TAK, Swapnil; BISEN, Gauri G.; SHIRSAT, Mahendra D., et al. *Effect of Thermal Annealing on an Emissive Layer Containing a Blend of a Small Molecule and Polymer as Host for Application in OLEDs.* Royal Society of Chemistry (RSC), -11-16, 2023 .
5. LIGUORI, Rosalba; NUNZIATA, Fiorita; APRANO, Salvatore and MAGLIONE, Maria G. *Overcoming Challenges in OLED Technology for Lighting Solutions.* MDPI AG, -03-30, 2024.
6. BANERJEE, Shrestha; SINGH, Piyush S.; PURKAYASTHA, Pradipta and KUMAR GHOSH, Sujit. *Evolution of Organic Light Emitting Diode (OLED) Materials and their Impact on Display Technology.* Wiley, -12-17, 2024.
7. CHIADMI, Yassine; CICEK, Paul-Vahe and IZQUIERDO, Ricardo. *Solution-Processed OLEDs: A Critical Review and Methodology Proposal for Stack Optimization.* MDPI AG, -02-05, 2026.
8. YIN, Da; JIA, Shi-Xin; ZHANG, Hao-Yang; LI, Su-Heng; LIU, Yue-Feng, et al. *Applications of Organic Light-Emitting Diodes in Wearable Electronics.* Elsevier BV, -07-12, 2025.
9. OH, Jun H.; SHIN, Jung G.; PODE, Ramchandra and KWON, Jang H. Achieving Highly Stable Tandem Organic Light-Emitting Diodes using Interfacial Property Control of Charge Generation Layer. Elsevier BV, -06-23, 2025.
10. YANG, Xiaoxue; MU, Ge; WENG, Kangkang and TANG, Xin. *Advances in High-Efficiency Blue OLED Materials.* MDPI AG, -09-13, 2024.
11. LIAO, Hao-Sen; WANG, Bao-Yue; CHEN, Dong; CAO, Yi-Ming and LI, Xiao. *Blue Organic Multifunctional Fluorescent Materials for Efficient Full-Color and White Organic Light-Emitting Diodes.* Elsevier BV, -06-09, 2025.
12. DEORI, Upasana; NANDA, Gyana P.; MURAWSKI, Caroline and RAJAMALLI, Pachaiyappan. *A Perspective on Next-Generation Hyperfluorescent Organic Light-Emitting Diodes.* Royal Society of Chemistry (RSC), -10-08, 2024.
13. ANWER, Makhvela and YIN, Shiwei. *Recent Progress and Prospects of Inverted Singlet-Triplet Energy Gap (INVEST) Materials in OLEDs.* Elsevier BV, -05-29, 2025.
14. XIAO, Shengbing; GAO, Ying; WANG, Runze; LIU, Haichao; LI, Weijun, et al. *Highly Efficient Hybridized Local and Charge-Transfer (HLCT) Deep-Blue Electroluminescence with Excellent Molecular Horizontal Orientation.* Elsevier BV, -03-21, 2022.
15. JAYABHARATHI, Jayaraman; THANIKACHALAM, Venugopal and THILAGAVATHY, Shanmugam. *Phosphorescent Organic Light-Emitting Devices: Iridium Based Emitter Materials – an Overview.* Elsevier BV, -03-10, 2023.

16. LAN, Ying; LIU, Di; LI, Jiuyan; MEI, Yongqiang and TIAN, Houru. *Blue Heteroleptic Iridium(Iii) Complexes for OLEDs: Simultaneous Optimization of Color Purity and Efficiency*. Royal Society of Chemistry (RSC), -11-02, 2022.
17. KAMARAJ, Eswaran; KOLLI, Deepti; ABBURI, Ramarao; KHALID, Awais; HEGAZY, H. H., et al. *Purely Organic Room-Temperature Phosphorescent Materials for OLEDs: Molecular Design, Photophysics, and Device Strategies.* Elsevier BV, -01-24, 2026.
18. ZHOU, Zixing; XIE, Xiaoyu; SUN, Zhonglie; WANG, Xiao; AN, Zhongfu, et al. *Recent Advances in Metal-Free Phosphorescent Materials for Organic Light-Emitting Diodes.* Royal Society of Chemistry (RSC), 2023.
19. FAGNANI, Francesco; COLOMBO, Alessia; DRAGONETTI, Claudia; FONTANI, Mattia; ROBERTO, Dominique, et al. *Blue and Green Phosphorescent Organic Light-Emitting Diodes Based on Bis(Cyclometalated) Tetrahydrocurcuminate Iridium(III) Complexes.* MDPI AG, -11-27, 2025.
20. LEE, Ji H.; JOO, Chul W.; SUNG, Baeksang; WOO, Seung-Je; WOO, Seungwan, et al. *Highly Efficient Single Emitter White Phosphorescent Organic Light-Emitting Diodes Based on Pt(II) Emitters.* Royal Society of Chemistry (RSC), -07-17, 2023.
21. PALEM, Ramasubba R.; SHIMOGA, Ganesh; LEE, Soo-Hong; KIM, Hyun-Seok and BATHULA, Chinna. *Recent Advances in OLED Applications of TADF Materials with Decreased Singlet-Triplet Energy Gaps.* Elsevier BV, -02-09, 2026.
22. PAGADALA, L. N. S. L.; VAIDYANATHAN, Sivakumar and RAVVA, Mahesh K. *Rigidifying Donor–acceptor Frameworks Via C–C Interlocking to Modulate Excited-State Dynamics in HLCT Emitters.* Royal Society of Chemistry (RSC), -03-14, 2026.
23. LIU, Meiyan; LI, Chenglong; DUAN, Lian and ZHANG, Dongdong. *Recent Advances in Blue Multiple-Resonance Thermally Activated Delayed Fluorescence Materials and their Applications in Organic Light-Emitting Diodes.* Wiley, -11-17, 2025.
24. MUGHAL, Ehsan U.; NAEEM, Nafeesa; KAINAT, Syeda F.; ALMOHYAWI, Abdulaziz M.; QURBAN, Jihan, et al. *Advances in the Design of Thermally Activated Delayed Fluorescence Materials for High-Efficiency OLEDs.* Elsevier BV, -05-22, 2025.
25. CHENG, Tianlin; CHEN, Xi; ZHONG, Daokun; LIU, Jun; HUANG, Xiong, et al. *Achieving Fast Reverse Intersystem Crossing and High Electroluminescent Efficiencies in TADF Emitters with N-Phenylphthalimide (PhAI) as Electron-Acceptor Coupled with Single Electron-Donor.* Elsevier BV, -12-22, 2025.
26. KOTHAVALE, Shantaram; KIM, Seung C.; CHEONG, Kiun; ZENG, Songkun; WANG, Yafei, et al. *Solution-Processed Pure Red TADF Organic Light-Emitting Diodes with High External Quantum Efficiency and Saturated Red Emission Color*. Wiley, -02-23, 2023.
27. SHEN, Chenxi; HU, Ying; ZHOU, Siqian; HE, Ziquan; HAN, Junchao, et al. *Vacuum Thermal Evaporation for OLEDs: Fundamentals, Optimization, and Implications for Perovskite LEDs.* Wiley, -10-16, 2025.
28. MANFREDI, Riccardo; PRONTERA, Carmela T.; MARIANO, Fabrizio; PUGLIESE, Marco; MAGGIORE, Antonio, et al. *Optimization of Electron Transport Layer Inkjet Printing Towards Fully Solution-Processable OLEDs.* MDPI AG, -07-09, 2025.
29. KAÇAR, Rifat; SERIN, Ramis B.; UÇAR, Esin and ÜLKÜ, Alper. *A Review of High-End Display Technologies Focusing on Inkjet Printed Manufacturing.* Elsevier BV, -02-02, 2023.

30. FO, Wan-Zhen; LI, Jun; LEI, Yu-Xing; WEI, Bin and ZHANG, Zhi-Lin. *A Facile and Efficient Preparation Method for the Doped Light Emitting Layer in OLEDs: Blade-Coated Planar Source Evaporation.* Elsevier BV, -11-24, 2023.
31. ZHANG, Lveting; HU, Dehua; WANG, Shipan; PAN, Yuyu; TAN, Wenle, et al. *High-Efficiency Deep Blue OLEDs with Hot Exciton Materials as Emitters and Hosts.* Wiley, -05-02, 2025.
32. SIDDIQUI, Iram; KUMAR, Sudhir; TSAI, Yi-Fang; GAUTAM, Prakalp; Shahnawaz, et al. *Status and Challenges of Blue OLEDs: A Review.* MDPI AG, -09-08, 2023.
33. XIE, Dian; HAN, Pengbo; LI, Baoxi; PAN, Jianhui; OU, Ningyan, et al. *Modeling and Analysis of Exciton Dynamics on "Hot Exciton" Process in Blue Fluorescent Organic Light-Emitting Diodes.* Wiley, -04-26, 2025.
34. HE, Junwei; LOU, Jingli; LIU, Luyao; XIAO, Chenfa; MA, Bingzhu, et al. *Efficient and Stable Deep-Blue OLEDs Employing Hot-Exciton Emitters with Rapid Exciton Dynamics: Achieving High EQEs Over 9% at 10 000 Cd M −2 with CIE Y <0.046.* Wiley, -10-09, 2025.
35. WANG, Wenhui; BIAN, Jinkun; CHEN, Kaijin; LI, Chuying; LONG, Yubo, et al. *Achieving Record External Quantum Efficiency of 11.5 % in Solution-Processable Deep-Blue Organic Light-Emitting Diodes Utilizing Hot Exciton Mechanism.* Wiley, -05-27, 2024.
36. ZENG, Songkun; XIAO, Chen; ZHOU, Jiachun; DONG, Qiwei; LI, Qiuying, et al. *Deep Blue Emitter Based on Tris(Triazolo)Triazine Moiety with CIEy < 0.08 for Highly Efficient Solution-Processed Organic Light-Emitting Diodes Via Molecular Strategy of "Hot Excitons".* Wiley, -02-09, 2022.
37. LI, Huiyang; HUNG, Faan-fung; WU, Siping; QIU, Jiangzhen; LI, Cuijin, et al. *Deep Blue Tetradentate Pt(II) Emitter Coordinated with Fused Fluorenyl N-heterocyclic Carbene. High Efficiency, Narrow FWHM, and Superior Operational Lifetime LT95 of 290 H at 1000 Cd M−2.* Wiley, -02-07, 2025.
38. MEI, Yongqiang; LIU, Di; LI, Jiuyan and WANG, Jiahui. *Accelerating PLQY and RISC Rates in Deep-Blue TADF Materials with the Acridin-9(10H)-One Acceptor by Tuning the Peripheral Groups on Carbazole Donors.* Royal Society of Chemistry (RSC), -10-17, 2022.
39. RAJENDRAN, Vignesh; ERULAPPAN, Jeyasurya R. J. and THOMAS, K. R. J. *Strategies for Enabling RGB Emission in Fused Carbazole Derivatives.* Wiley, -05, 2025.
40. ONER, Saliha and BRYCE, Martin R. *A Review of Fused-Ring Carbazole Derivatives as Emitter and/Or Host Materials in Organic Light Emitting Diode (OLED) Applications.* Royal Society of Chemistry (RSC), -06-28, 2023.
41. XIMENES, Matheus C.; FERREIRA, Jorge L. M.; DE SOUZA, Ana P. N.; TOMASO, Luiz P. D. S.; DA SILVA, Gabriel F. S., et al. *Organic Electronics: Basic Fundamentals and Recent Applications Involving Carbazole-Based Compounds.* MDPI AG, -12-23, 2024.
42. GUO, Ting; LIU, Zhangshan; JIANG, Ruming; TANG, Ben Z. and ZHAO, Zujin. *Efficient Deep-Blue Fluorescent Material Serving as Emitter and Host for High-Performance Organic Light-Emitting Diodes.* Science Exploration Press, -01-09, 2025.
43. SUN, Mizhen; WANG, Runze; MA, Chenglin; ZHOU, Yannan; WANG, Xin, et al. *Efficient Near-Ultraviolet OLED Utilizing a Novel Emitter Based on Fluorene Bridge with Subtlety Stacking Patterns.* Elsevier BV, -02-08, 2025.

44. KEERTHIKA, P.; KUMAR, Ankit; MARUTHAPILLAI, Arthanareeswari; NUTALAPATI, Venkatramaiah and KONIDENA, Rajendra K. *Recent Advances in the Molecular Designs of Near Ultraviolet Emitters for Efficient Organic Light Emitting Diodes*. Elsevier BV, -04-23, 2025.
45. QU, Yunzhuo and LI, Yuanzhe. *Structural Insights and Molecular Advancements in Fluorene-Based Electroluminescent Materials: A Mini-Review*. Elsevier BV, -01-15, 2025.
46. LEE, Changjun; PARK, Sangwook; KWON, Hyukmin; LEE, Hayoon and PARK, Jongwook. *High Efficiency and Long Device Lifetime of Organic Light-Emitting Diodes using New Electron-Transporting Materials with Spirobifluorene Groups*. Elsevier BV, -04-21, 2025.
47. SICARD, Lambert; BROUILLAC, Clément; LECLERC, Nicolas; FALL, Sadiara; ZIMMERMAN, Nicolas, et al. *Influence of the Pendant Substituent at the C1 Position of a Spirobifluorene Scaffold on the Electronic Properties*. Royal Society of Chemistry (RSC), -01-01, 2024.
48. KANG, Ji A.; LIM, Junseop and LEE, Jun Y. *Spirobifluorene Modified Electron Transport Materials for High Efficiency in Phosphorescent Organic Light-Emitting Diodes*. Royal Society of Chemistry (RSC), -01-25, 2022.
49. HE, Zhanhui; LIU, Zheng; LI, Hongji; YANG, Lijun; YIN, Guodong, et al. *Synthesis of Multi-Substituted 9,9'-Spirobifluorenes and their Applications in Organic Light-Emitting Diodes*. Elsevier BV, -11-22, 2025.
50. SUN, Yufu; FU, Xi-feng; HOU, Chen-lu; ZHANG, Dong-hai; HU, Jia-xuan, et al. *Multifunctional Hot-Exciton Fluorophore Enabling Efficient Non-Doped Blue Electron-Fluorescence with Negligible Efficiency Roll-Off and Phosphorescent OLEDs with Ultra-Low Power Consumption*. Wiley, -03-28, 2025.
51. ZHANG, Lveting; LI, Mingke; WANG, Shipan; NIU, Pengfei; TAN, Wenle, et al. *Dibenzofuran-Based Blue Hot Exciton Materials as Hosts: Enabling High-Efficiency and Long-Lifetime Solution-Processed OLEDs*. Elsevier BV, -02-03, 2026.
52. LEE, Changjun; PARK, Sangwook; KWON, Hyukmin; LEE, Hayoon and PARK, Jongwook. *High Efficiency and Long Device Lifetime of Organic Light-Emitting Diodes using New Electron-Transporting Materials with Spirobifluorene Groups*. Elsevier BV, -04-21, 2025.
53. BERESNEVICIUTE, Raminta; BLAZEVICIUS, Dovydas; GRIGALEVICIUS, Saulius; HE, Zih-Ru; YANG, Fong-Yu, et al. *Versatile Carbazole and Dibenzofuran-Based Materials for OLEDs: Emitters and Exciplex-Forming Systems*. Elsevier BV, -05-14, 2025.
54. LI, Linjie; LI, Jiaqi; GUO, Lixiao; XU, Yincai; BI, Yifan, et al. *A Multi-Resonance Emitter with Five-Membered Thiophene as the ΠΤ-Core Enables Efficient, Narrowband and Reduced Efficiency Roll-Off OLEDs*. Royal Society of Chemistry (RSC), -06-18, 2024.
55. JIANG, Ruming; LIU, Zhangshan; HAN, Yuanyuan; LONG, Jiawei; GUO, Ting, et al. *Introducing Electron-Rich Thiophene Bridges in Hot Exciton Emitter for Efficient Non-Doped Near-Infrared OLEDs with Low Turn-on Voltages*. Elsevier BV, -11-12, 2024.
56. GANCZARCZYK, Roman; RYBAKIEWICZ-SEKITA, Renata; ZAWADZKA, Magdalena; PANDER, Piotr; LEDWON, Przemysław, et al. *The Impact of Structural Modification on the Electrochromic and Electroluminescent Properties of D–A–D Benzothiadiazole Derivatives with a Fluorene Linker and (Bi)Thiophene Units*. Royal Society of Chemistry (RSC), -09-02, 2024.

57. YANG, Xiaoxue; MU, Ge; WENG, Kangkang and TANG, Xin. *Advances in High-Efficiency Blue OLED Materials.* MDPI AG, -09-13, 2024.
58. STARYKOV, Hryhorii; BEZVIKONNYI, Oleksandr; LEITONAS, Karolis; SIMOKAITIENE, Jurate; VOLYNIUK, Dmytro, et al. Derivatives of Phenyl Pyrimidine and of the Different Donor Moieties as Emitters for OLEDs. MDPI AG, -03-15, 2024.
59. KALATOZISHVILI, Akaki; KERUCKIENE, Rasa; NAGHIZADE, Rashad; BEZVIKONNYI, Oleksandr; VOLYNIUK, Dmytro, et al. Hole-Transporting Deep Blue Emissive Derivatives of Fluorene and Dibenzofuran Or Carbazole for Organic Light Emitting Diodes. Elsevier BV, -03-04, 2026.
60. DVYLYS, Lukas; KERUCKIENE, Rasa; GUZAUSKAS, Matas; LEITONAS, Karolis; SADZEVICIENE, Rita, et al. Exploring Donor-Acceptor Derivatives of Quinoxaline-6-Carbonitrile a Strategy for Efficient Orange OLEDs Via Tunable Photophysical Properties. Elsevier BV, -01-10, 2026.
61. YANG, Jie; FANG, Manman and LI, Zhen. Organic Luminescent Materials: The Concentration on Aggregates from Aggregation-induced Emission. Wiley, -12, 2020.
62. FENG, Weiqiang; SU, Qiang; MA, Yao; DŽOLIĆ, Zoran; HUANG, Fei, et al. *Tetraphenylbenzosilole: An AIE Building Block for Deep-Blue Emitters with High Performance in Nondoped Spin-Coating OLEDs.* American Chemical Society (ACS), -11-12, 2019.
63. ZHANG, Dongdong; CAI, Minghan; ZHANG, Yunge; ZHANG, Deqiang and DUAN, Lian. *Sterically Shielded Blue Thermally Activated Delayed Fluorescence Emitters with Improved Efficiency and Stability.* Royal Society of Chemistry (RSC), 2016.
64. KAMATA, Takahiro; SASABE, Hisahiro; ITO, Nozomi; SUKEGAWA, Yoshihito; ARAI, Ayato, et al. *Simultaneous Realization of High-Efficiency, Low-Drive Voltage, and Long Lifetime TADF OLEDs by Multifunctional Hole-Transporters.* Royal Society of Chemistry (RSC), -05-01, 2020.
65. Law ot the Republic of Lithuania on Safety and Health at Work, No. IX-1672 of 1 July 2003. https://e-seimas.lrs.lt/portal/legalAct/lt/TAD/TAIS.215253?jfwid=j1u6bxt4x
66. Bendrosios gaisrinės saugos taisyklės. Valstybės žinios, 2010, Nr. 99 -5167 (Aktuali redakcija: Valstybės žinios Nr. 118-5970)
67. HN 69:2003. Šiluminis komfortas ir pakankama šiluminė aplinka darbo patalpose. Parametrų norminės vertės ir matavimo reikalavimai. Valstybės žinios, 2004, Nr. 45-1485
68. HN 33:2011. „Triukšmo ribiniai dydžiai gyvenamuosiuose ir visuomeninės paskirties pastatuose bei jų aplinkoje“. Valstybės žinios, 2011, Nr. 75-3638
69. HN 23:2011. Cheminių medžiagų profesinio poveikio ribiniai dydžiai. Matavimo ir poveikio vertinimo bendrieji reikalavimai. Valstybės žinios, 2011, Nr. 112-5274
70. HN 98:2014. Natūralus ir dirbtinis darbo vietų apšvietimas. Apšvietos ribinės vertės ir bendrieji matavimo reikalavimai. TAR, 2014, Nr. 5119
71. Elektros įrenginių įrengimo taisyklės. Vilnius, 2000. 487 p
72. Lietuvos Respublikos ūkio ministro įsakymas Nr. 40 „Dėl Saugos taisyklių eksploatuojant elektros įrenginius DT 11-02 patvirtinimo“,202m.vasario 5d., Valstybės žinios, 2002, Nr. 27-974
73. Specialiųjų patalpų ir technologinių procesų elektros įrenginių įrengimo taisyklės. Valstybės žinios, 2013, Nr. 27-1299